European Journal of Cell Biology 103 (2024) 151425

Contents lists available at ScienceDirect

European Journal of Cell Biology

journal homepage: www.elsevier.com/locate/ejcb

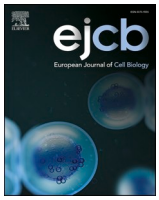

RAS isoform specific activities are disrupted by disease associated mutations during cell differentiation

Rohan Chippalkatti [1], Bianca Parisi [1], Farah Kouzi, Christina Laurini, Nesrine Ben Fredj, Daniel Kwaku Abankwa [*]

Cancer Cell Biology and Drug Discovery group, Department of Life Sciences and Medicine, University of Luxembourg, Esch-sur-Alzette 4362, Luxembourg

ARTICLE INFO

Key words:
Ras
Cancer
RASopathy
Flow cytometry
Inhibitors
Differentiation

ABSTRACT

The RAS-MAPK-pathway is aberrantly regulated in cancer and developmental diseases called RASopathies. While typically the impact of Ras on the proliferation of various cancer cell lines is assessed, it is poorly established how Ras affects cellular differentiation. Here we implement the C2C12 myoblast cell line to systematically study the effect of Ras mutants and Ras-pathway drugs on differentiation. We first provide evidence that a minor pool of Pax7+ progenitors replenishes a major pool of transit amplifying cells that are ready to differentiate. Our data indicate that Ras isoforms have distinct roles in the differentiating culture, where K-Ras depletion increases and H-Ras depletion decreases terminal differentiation. This assay could therefore provide significant new insights into Ras biology and Ras-driven diseases. In line with this, we found that all oncogenic Ras mutants block terminal differentiation of transit amplifying cells. By contrast, RASopathy associated K-Ras variants were less able to block differentiation. Profiling of eight targeted Ras-pathway drugs on seven oncogenic Ras mutants revealed their allele-specific activities and distinct abilities to restore normal differentiation as compared to triggering cell death. In particular, the MEK-inhibitor trametinib could broadly restore differentiation, while the mTOR-inhibitor rapamycin broadly suppressed differentiation. We expect that this quantitative assessment of the impact of Ras-pathway mutants and drugs on cellular differentiation has great potential to complement cancer cell proliferation data.

1. Introduction

Malignant tumors are characterized by abnormal proliferation and invasive growth of dedifferentiated tissue. The Ras-pathway is central to control cellular proliferation, differentiation and survival, and is dysregulated in virtually every cancer (Crespo and Leon, 2000; Hanahan, 2022). Three *RAS* genes, *KRAS*, *NRAS* and *HRAS,* are mutated in 19% of human cancers making *RAS* the most frequently mutated oncogene (Prior et al., 2020). Out of the two *KRAS* splice isoforms, K-Ras4A and K-Ras4B, the latter is the highest expressed isoform and the major focus of current drug development (Hood et al., 2023; Moore et al., 2020; Tsai et al., 2015).

Ras membrane association is required for its activity, and membrane affinity is mediated by C-terminal lipid modifications of Ras by farnesyltransferase and palmitoyltransferases (Pavic et al., 2022). Farnesylation also mediates binding of Ras to trafficking chaperones, such as PDE6D and calmodulin, which facilitate its diffusion, followed by trapping on secretory organelles, and subsequent vesicular transport to the plasma membrane (Schmick et al., 2015).

Canonical Ras signaling emerges at the plasma membrane, where extracellular mitogens activate receptor tyrosine kinases, such as epidermal growth factor receptor (EGFR), which indirectly relays its activation to guanine nucleotide exchange factors (GEFs), such as SOS. GEFs facilitate exchange of GDP for GTP, thus activating Ras. The active GTP-bound Ras then recruits effector proteins, such as Raf, PI3K and RalGDS from the cytosol to the membrane, leading to their activation (Simanshu et al., 2017). Raf-kinases trigger the MAPK-pathway, which includes activation of downstream kinases MEK and ERK, the latter of which leads to well characterized changes that drive the cell cycle and thus proliferation (Crespo and Leon, 2000). The effector PI3K activates the kinase Akt, which further downstream engages the mTORC1-pathway and thus cell growth and many other crucial cellular

* Corresponding author.
E-mail address: daniel.abankwa@uni.lu (D.K. Abankwa).
[1] These authors contributed equally

https://doi.org/10.1016/j.ejcb.2024.151425
Received 13 February 2024; Received in revised form 2 May 2024; Accepted 21 May 2024
Available online 22 May 2024

processes (Laplante and Sabatini, 2013). Ras can furthermore activate mTORC2, which phosphorylates Akt on Ser473 (Kovalski et al., 2019).

The active state of Ras is tightly regulated, with GTP-Ras becoming inactivated by GTPase-activating proteins (GAPs) (Simanshu et al., 2017). The most prominently studied GAP is neurofibromin 1 (NF1), which is recruited by B-Raf and one of three SPRED proteins to K-Ras nanodomains of the plasma membrane (Siljamaki and Abankwa, 2016; Stowe et al., 2012; Yan et al., 2020). Landmark structural data from the mid 1990s already explained how hotspot oncogenic mutations in codons 12 and 61 of Ras disable the GTP-hydrolysis of Ras by NF1 and other arginine-finger GAPs (Ahmadian et al., 1997; Scheffzek et al., 1997). However, the heterotrimeric G protein GAP RGS3 with a catalytic asparagine, was recently shown to facilitate GTP-hydrolysis of all major oncogenic K-Ras mutants (G12D/V, G13C/D) (Li et al., 2021), suggesting that a distinct function of NF1 is disabled by oncogenic Ras.

In line with the mitogen-independent mutational activation of Ras, cancer cell assays typically assess the uncontrolled cell growth. Proliferation assays provided a wealth of data in cancer research, such as from large scale genetic and chemical screens (Barretina et al., 2012; McDonald et al., 2017; Tsherniak et al., 2017). However, among pathologists it is well established that dedifferentiation is the most unsettling hallmark of cancer (Chaffer and Weinberg, 2015; Hanahan, 2022). Unfortunately, the functions of Ras during cellular differentiation are only poorly understood and typically not assayed.

This lack of understanding also impacts on the treatment development for another type of Ras-driven diseases. Germline mutations in the RAS-MAPK-pathway lead to individually rare but collectively common developmental syndromes called RASopathies, which are characterized by facial malformations, short stature, cutaneous defects, cardiac hypertrophy and a pre-disposition to cancer (Castel et al., 2020; Rauen, 2013). They illustrate how even a mild overactivation of the MAPK-pathway during embryonal development perturbs proper differentiation in multiple organ systems.

For instance, the RASopathy Noonan syndrome can be caused by the *KRAS-D153V* mutation, which in contrast to cancer-associated hotspot mutations, is still sensitive to the GAP NF1, but shows mildly increased effector binding (Gremer et al., 2011). Loss-of-function mutations in *NF1* itself lead to neurofibromatosis type I, one of the more common RASopathies (Rauen, 2013). This disorder shares some phenotypic similarities with the very rare RASopathy Legius syndrome, which is caused by heterozygous loss-of-function mutations in the *SPRED1* gene (Brems et al., 2012). To analyze RASopathy mutants, dedicated low-throughput assays have been developed, which characterize early developmental defects during gastrulation or later in the whole organism in zebrafish and mouse animal models (Jindal et al., 2015). Yet, insufficient developmental or cell differentiation assay capacities may underlie the lack of efficacious therapies for most RASopathies (Gross et al., 2020).

These observed developmental defects in RASopathies are consistent with the deep integration of MAPK-signaling already at the level of stem cell maintenance. During organismal development, pluripotent stem cells give rise to a vast variety of differentiated tissues (Morrison and Kimble, 2006). Both during priming of naïve mouse embryonic stem cells and maintenance of pluripotency in human induced pluripotent stem cells is the MAPK-pathway involved (Altshuler et al., 2018; Haghighi et al., 2018). In the fully developed organism, adult stem and progenitor cells are important for tissue homeostasis. They typically divide asymmetrically, giving rise to one stem cell (referred to as self-renewal) and one committed or differentiated cell (Morrison and Kimble, 2006).

The C2C12 cell model is one of the best characterized *in vitro* differentiation systems, which recapitulates essential *in vivo* processes (Yin et al., 2013). This cell line was derived from a skeletal muscle of a 2-month old mouse, and is typically considered a heterogenous population of myoblasts (myogenic progenitor cells), which proliferate and remain undifferentiated under high serum conditions (Bennett and Tonks, 1997). Mitogen withdrawal in low serum culture conditions, rapidly triggers terminal differentiation of the majority of C2C12 cells into multinucleated myotubes within five days (Bennett and Tonks, 1997).

However, it is known that a small fraction of proliferating C2C12 cells expresses the muscle progenitor marker Pax7, a paired box transcription factor, as well as the basic helix-loop-helix transcription factor Myf5 (Yoshida et al., 1998). Differentiating cells downregulate Pax7 and upregulate myogenic factors, such as MyoD, myogenin and subsequently late differentiation markers, such as the motor protein myosin II heavy chain (MyHC) (Brown et al., 2012; Olguin and Olwin, 2004). Interestingly, upon serum withdrawal a minor fraction remains undifferentiated and continues to express the progenitor marker Pax7, but no MyoD, Myf5 or myogenin (Olguin and Olwin, 2004; Yoshida et al., 1998). These features strikingly resemble quiescent satellite cells, the Pax7 positive adult stem cell population in muscles (Yablonka-Reuveni and Rivera, 1994). Currently, it is not fully resolved, how the minor fraction of myoblast progenitors is connected to a major fraction of differentiated cells.

Myogenic differentiation is initiated by a rapid upregulation of SPRED1 upon serum switching and a subsequent decrease in MAPK-signaling (Bennett and Tonks, 1997; Wakioka et al., 2001). In line with mitogens maintaining proliferation of myoblasts, oncogenic Ras prevents myogenic differentiation by downregulating the myogenic transcription factor MyoD and myogenin (Lassar et al., 1989). Conversely, overexpression of tumor suppressors, such as Sprouty2 and SPRED1 stimulate myogenesis even under high serum conditions (de Alvaro et al., 2005; Wakioka et al., 2001). Terminal differentiation is then promoted by mTORC2-Akt activity (Shu and Houghton, 2009).

The proper differentiation trajectories of tissues is perturbed in cancer and may lead to the emergence of rare cancer stem cells, which alone have the potential to seed new tumors, for example during metastization and relapse after therapy (Morrison and Kimble, 2006). Current cancer stem cell models suggest either reprogramming of differentiated cells or an evolution directly from transformed stem/progenitor cells (Ansieau, 2013; Batlle and Clevers, 2017). Cancer stem cells are best characterized in functional and lineage tracing assays *in vivo* (Nassar and Blanpain, 2016). Yet, *in vitro* surrogate assays persist, such as flow cytometry based detection of cancer stem cell markers (e.g., CD44+/CD24-), or of cancer stem cells in the side population, which is characterized by their increased drug efflux properties (Golebiewska et al., 2011; Li et al., 2017). In addition, low serum, non-adherent 3D spheroid cultures of human mammary stem/ progenitors cells, called mammospheres, were originally employed to maintain and study such cells in culture (Dontu et al., 2003). Subsequently these culture conditions were widely adopted to monitor cancer cell stemness from tumorospheres (Weiswald et al., 2015). The simplicity of this assay enabled screening for compounds that may have a potential to target specifically cancer stem cells (2022; Mathews et al., 2012; She et al., 2021).

Current data suggest that *KRAS* is the strongest driver of stemness features, followed by *NRAS* and then *HRAS* (Najumudeen et al., 2016; Quinlan et al., 2008; Wang et al., 2015). This potency order that was obtained across multiple model systems strikingly correlates with the *RAS* mutation frequency in cancer (Chippalkatti and Abankwa, 2021). Salinomycin was one of the first cancer stem cell selective inhibitors that was described by the Weinberg group (Gupta et al., 2009). This and related compounds showed selective activity against K-Ras, but not H-Ras, suggesting that K-Ras is of high significance in cancer stem cells (Najumudeen et al., 2016; Okutachi et al., 2021; Siddiqui et al., 2021). While these natural products may become starting points for the development of more potent drugs, they contrast with dedicated inhibitors raised against the target K-Ras. Two such inhibitors, sotorasib (AMG 510) and adagrasib (MRTX849) have recently been approved (Canon et al., 2019; Fell et al., 2020). Essentially all of these covalent K-Ras-G12C specific inhibitors were built on the development of the compound ARS-1620 (Janes et al., 2018). Moreover, MRTX849

derivatives gave rise to other non-covalent inhibitors, including MRTX1133 against K-Ras-G12D (Wang et al., 2022). While allele specific inhibitors promise uniquely small side-effects, their limited applicability necessitates the development of innovative K-Ras inhibitors with new modes of action (Steffen et al., 2023).

Here we utilized mainly flow cytometry-based differentiation marker quantification to understand the impact of the three Ras isoforms, notably K-Ras4B, on C2C12 cell differentiation. We first establish a new baseline of understanding C2C12 cell differentiation, by elaborating that Pax7+ progenitors replenish a major pool of Pax7- transit amplifying cells, which then give rise to the MyHC+ differentiated cells.

We then establish the distinct impact of Ras isoforms on differentiation using specific genetic perturbations. Finally, we demonstrate the applicability of our assay for medium throughput assessment of Ras-pathway drugs to restore differentiation that was perturbed by disease-associated Ras-isoforms and -alleles. Our results demonstrate how profoundly Ras-isoforms impact on cell differentiation and demonstrate how to rapidly analyze the effect of Ras-mutants and -drugs on differentiation.

2. Materials and methods

2.1. Materials and resources

A list of all reagents, software and instrumentation used in this study together with their sources and identifiers is provided in Table S1.

2.2. Cell culture and transfections

C2C12 cells were maintained in Dulbecco's modified Eagle Medium (DMEM) supplemented with ~9% (v/v) fetal bovine serum (FBS), 2 mM L-glutamine and 1% penicillin/streptomycin (high serum culture medium). Cells were incubated in a humidified incubator at 37 °C, with 5% CO_2 and passaged when reaching 50 – 60% confluency. Passage numbers are indicated in the legends and passages beyond ten were not employed. Cell culture medium was exchanged with DMEM supplemented with ~2% horse serum (HS), 2 mM L-glutamine and 1% penicillin/streptomycin (low serum culture medium) to induce differentiation at 90% confluency. For experiments lasting three to five days fresh low serum culture medium was added every day.

2.3. Preparation of expression constructs

Plasmid constructs used for transfection were generated by multisite gateway cloning (Wall et al., 2014). To generate the final expression constructs, LR Clonase II enzyme mix was used to perform recombination of the entry clones encoding the promoter, the fluorescent tag and the gene of interest with the pDest-305 destination vector. The reaction mix was transformed into ccdB-sensitive *E. coli* strain DH10B. Colonies resistant to ampicillin were selected for screening of their plasmid DNA by restriction digestion with BsrGI-HF enzyme. Plasmids with the expected fragment sizes were then further validated by sequencing. The pmEGFP-KRas4B-G12V-S17N construct was generated by site directed mutagenesis on the pmEGFP-KRas4B-G12V background by Gene Universal (Delaware, USA).

2.4. Plasmid DNA transfection

C2C12 cells were seeded in high serum medium at a density of 100,000 cells per mL of a 6-well plate (#10062–892, Avantor) and transfection was performed after the cells reached 50 – 60% confluency (typically 24 h after seeding). Transfection was performed according to the protocols provided by the manufacturer. 2 μg of plasmid DNA and 7.5 μL Lipofectamine 2000 were added to 250 μL Opti-MEM medium. The mixture was vortexed, incubated at 22–25 °C for 10 min and subsequently added dropwise to one well of a 6-well plate. Medium was exchanged with fresh high serum medium after 4 h. After further 24 h incubation with high serum, medium was exchanged with low serum medium to induce differentiation.

2.5. Knockdown by siRNA transfection

Any siRNAs were transfected using Lipofectamine RNAiMAX diluted in Opti-MEM medium. Typically, 100 nM of each siRNA and 7.5 μL of Lipofectamine were added to 250 μL of Opti-MEM medium, mixed and incubated at 22 – 25 °C for 10 min. Cells were transfected at 50 – 60% confluency by adding this mixture. After 24 h of incubation with the siRNA-Lipofectamine mixture, the medium was substituted with fresh high serum medium. After 3 – 4 h, high serum medium was exchanged with low serum medium, and cells were cultured in low serum medium that was replaced every day.

2.6. Antibody conjugation with Allophycocyanin (APC) or Phycoerythrin (PE)

For flow cytometry experiments anti-Pax7 and anti-myogenin antibodies were conjugated to APC with the reagents provided in the APC conjugation kit – Lightning link. Anti-Myosin 4 Monoclonal antibody (anti-MyHC) was conjugated with PE with the components provided in the PE/R-Phycoerythrin conjugation kit – Lightning link. The modifier reagent and quencher reagent were contained in both kits. Additionally, the APC conjugation reaction mix was supplied with the APC kit and the PE conjugation reaction mix was supplied with the PE/R-Phycoerythrin kit. Anti-Pax7 or anti-myogenin antibodies at a concentration of 1 mg/mL and 100 μL volume were mixed with 100 μg APC Conjugation Reaction Mix, together with 10 μL of Modifier Reagent. Similarly, 100 μL of 0.5 mg/mL anti-MyHC antibody was mixed with 100 μg PE Conjugation Reaction Mix with 10 μL of Modifier Reagent. This mixture was stored in the dark at 22 – 25 °C for 3 – 4 h. Subsequently, the conjugation reaction was stopped by adding 10 μL quencher reagent to the conjugation mix. The conjugated antibody solution was used at a dilution of 1:100 and stored at 4 °C for up to 6 months.

The degree of labelling (DOL) was calculated according to the formula, DOL = (Amax × MW × dilution factor)/(ε × [conjugate]). MW is the molecular weight of IgG (~150,000 g/mol), and ε is the molar extinction coefficient of the dye (e.g. 700,000 M^{-1} cm^{-1} for APC), [conjugate] = ((A280 – (Amax × Cf))/1.4) × dilution factor. Here, [conjugate] is the concentration in mg/ mL of the antibody conjugate, 'dilution factor' is the fold of dilution used for spectral measurements. A280 is the absorbance of the conjugate at 280 nm and Amax is the absorption maximum of APC. Cf is the absorbance correction factor and the value 1.4 is the extinction coefficient of IgG in mg/mL. For APC, Cf is 0.22. We obtained 0.5 – 1 moles of APC per antibody, which falls within the optimal range for labelling. Similar results were obtained with the PE conjugation kit.

2.7. Flow cytometry

Cells were seeded at a concentration of 100,000 cells/mL per well of a 6-well plate. This was followed by transfection with the required plasmids or siRNAs and a low serum culture period for the time indicated in the figures or figure legends. Fresh low serum, where required with drug/ compound, was added every day. Cells were then harvested by trypsinization with 0.05% (w/v) trypsin EDTA (1×) for 5 min and pelleted by centrifugation at 500 × g for 5 min. The subsequent steps were performed at 22–25 °C. The cell pellet was subsequently fixed with 4% (w/v) paraformaldehyde (PFA) in PBS for 10 min. After washing with PBS, cells were permeabilized with 0.5% (v/v) Triton X-100 in PBS for 10 min. Subsequently cells were washed with 0.05% (v/v) Tween 20 in PBS (PBST) and immunolabelled with fluorescent dye-conjugated primary antibodies at the indicated dilutions in PBST for 1 h at 4 °C. Subsequently cells were pelleted by centrifugation at 500 × g for 5 min

and resuspended in PBST for flow cytometric analysis.

We first gated around 30,000 cells based on their forward and side scatter properties to exclude debris or dead cells. The intact cells thus obtained were further analyzed for expression markers using dot plots. In general, 1,000 to 10,000 EGFP-variant construct expressing intact cells were collected, depending on the treatment condition. Predominantly, mEGFP-tagged constructs were employed, which have the identical brightness as EGFP-tagged constructs (Norris et al., 2015). EGFP-variants and Alexa Fluor 488 were excited with the 50 mW photodiode 488 nm laser and the fluorescent signal was detected using the Green-B filter (band pass 525/30 nm) on a Guava Luminex easyCyte 6HT 2 L flow cytometer. APC or eFluor 660 were excited using the 100 mW photodiode 642 nm laser and detected using the Red-R filter (band pass 662/15 nm). PE was excited using the 50 mW photodiode 488 nm laser and detected using the Yel-B filter (band pass 583/26 nm). An unlabeled sample was always included as a control to correct for autofluorescence. Spectral overlap of PE and EGFP was corrected via digital compensation using single color EGFP-only and PE-only control samples.

Labelled or EGFP-variant expressing cells were quantified using the 'Quad Stat plot' feature on the GuavaSoft 4.0 software. The laser power and the voltage gain settings were adjusted such that the unlabeled events appeared below the level of 10^1 relative fluorescence units (RFU). Two EGFP-expression windows were defined, 'GFP low' between 10^1 and 10^2 RFU and 'GFP high' between 10^2 and 10^5 RFU. This allowed to quantitate differentiation in dependence of the EGFP-expression level. The majority of data were analyzed in the GFP low window, which produced a phenotype comparable to non-transfected C2C12 cells. A detailed step-by-step procedure of sample preparation, data acquisition and analysis is described in our previous work (Parisi et al., 2023).

To visualize the changes in Pax7+, myogenin+ and MyHC+ cell fractions over time, histograms depicting the fluorescence intensities of marker-labelled populations were generated with the Overlays tool in FlowJo.

To evaluate drug-induced cell toxicity, gating was applied based on forward and side scatter characteristics to separate total events into intact cells and debris. The percentage of intact cells among the total events was then plotted for each EGFP-construct and drug treatment to estimate cell toxicity.

2.8. Cell proliferation analysis in dye dilution experiments

A 500 × stock solution of Cytopainter deep red/Cytopainter orange was prepared as described by the manufacturer and stored at -20°C. A 1 × working solution was prepared on the day of labelling in Hank's balanced salt solution (HBSS). Cells from a confluent flask were detached with trypsinization, pelleted by centrifugation at 200 × *g* for 3 min and 1 mL high serum medium was added to the pellet. Cells were then counted on a Z1 particle counter (Beckman Coulter) to obtain 100,000 cells per 1 mL high serum medium. Cells were again pelleted by centrifugation at 500 × *g* for 5 min, resuspended in 500 μL cytopainter working solution and incubated in the dark at 37 °C for 15 min. Cells were once more pelleted (500 × *g* for 5 min) and the pellet was washed once with 500 μL HBSS. After another round of pelleting, cells were finally resuspended in 1 mL high serum medium. 200 μL from this cell suspension was kept aside as the day 0 followed by fixation with 4% (w/v) PFA. Out of the remaining 800 μL, 200 μL cell suspension containing 20,000 cells was dispensed per well in 3 wells of a 6-well plate containing 2 mL high serum medium. Cells were then incubated for 3 days in the cell culture incubator. Cells from one well were collected by trypsinization on day 1, day 2 and day 3 and processed for immunofluorescence with mouse monoclonal anti-Pax7, Alexa Fluor 488 antibody. Cytopainter deep red fluorescence was detected by 642 nm laser excitation and using the Red-R emission filter (band pass 661/15 nm). The half-life ($t_{1/2}$) of the cytopainter dilution was calculated using the one-phase decay equation in Prism 9.0, $Y = (Y0 - \text{plateau}) \times \exp(-K \times X) + \text{plateau}$. Here, X is time (days), Y is the cytopainter mean fluorescence intensity, Y0 is the Y value at day 0 which decays with one phase to plateau and K is the rate constant expressed as a reciprocal of the X axis unit. The $t_{1/2}$ value was calculated as ln(2)/K.

The 'Misc parameters' feature on the GuavaSoft software provides the number of events per μL of each sample, which allowed us to calculate the cell concentration per mL of Pax7+ and Pax7- fractions. To analyze cell proliferation in cells transfected with mEGFP-tagged wt K-Ras or K-RasG12V constructs, 100,000 cells/ mL were first seeded in all wells of a 6-well plate. Each construct was transfected in all wells of a 6-well plate. Transfected cells were then harvested by trypsinization, cells from all wells were pooled in a single 15 mL falcon tube and cell concentration was determined with a Z1 particle counter. Cell staining with cytopainter orange reagent was then carried out in exactly as described above for cytopainter deep red. Cells labelled with cytopainter orange were then fixed and immunolabelled with APC conjugated anti-Pax7 antibody. Cytopainter orange fluorescence was detected with 488 nm laser excitation and the Yel-B emission filter (band pass 583/26 nm). Cytopainter orange fluorescence signal for Pax7+ and Pax7- fractions was measured specifically for cells in the 'GFP low' window.

2.9. Cell toxicity analysis with 7-AAD

The cell impermeable dye 7-Aminoactinomycin D (7-AAD) is excluded from intact cells but intercalates into the genomic DNA of late apoptotic and necrotic cells since the plasma membrane integrity of these cells is compromised. The toxicity of K-RasG12C inhibitors was analyzed in cell fractions transfected with pDest305-CMV-mEGFP-K-RasG12C. Cells were treated 24 h after transfection with DMSO, sotorasib (AMG 510), MRTX1257 and adagrasib (MTRX849) in low serum for three days at indicated concentrations. The medium was first aspirated from drug treated cells to collect the 'supernatant' fraction of dead cells. The 'adherent' fraction of cells was collected by trypsinization. After centrifugation at 500 × *g* for 5 min and a washing step with PBS, both fractions were labelled with the provided 7-AAD solution for 15 min on ice according to the manufacturer instructions. The 7-AAD fluorescence was detected using the 100 mW photodiode 642 nm laser and the Red-B filter (band pass 635/40 nm) by flow cytometry. Cells expressing EGFP-constructs and labelled with 7-AAD were gated and counted using the Quad Stat plot feature on GuavaSoft software. Percentages of GFP+ 7AAD+ cells were quantified from the GFP low window and plotted for each drug treatment.

2.10. Microscopy

Brightfield images were acquired with 10 and 20 × objectives of a Leica DMI3000 B inverted microscope equipped with a Leica DFC360 FX digital camera. Samples were illuminated using pE400max LED white light source from CoolLED. Images were analyzed with Leica LAS X software.

2.11. Immunoblotting

Cells were seeded at a density of 100,000 cells/ mL in each well of a 6-well plate, transfected and then cultured in low serum as indicated in the figures. Cells were then washed with ice-cold PBS and lysed for 30 min on ice using a total of 100 μL of lysis buffer (10 mM Tris pH 7.5, 150 mM NaCl, 0.5 mM EDTA, 0.2% NP40) supplemented with one tablet of protease inhibitor cocktail per 10 mL lysis buffer. The lysis buffer was additionally supplemented with one tablet per 10 mL of the PhosSTOP phosphatase inhibitor cocktail. Cells were collected using a scraper and incubated on ice for 30 min with intermittent vortexing. Lysates were cleared by centrifugation at 13,000 × *g* for 10 min at 4 °C. Supernatants were collected and quantified by the Bradford assay using Bio-Rad Protein Assay Kit, followed by heating at 95 °C for 5 min. Protein samples were then resolved on denaturing SDS-PAGE. A 6% resolving

gel was used for detection of MyHC, 10% resolving gel for Pax7, ERK1/2, Akt and 15% resolving gel for detection of myogenin, K-Ras (total K-Ras, both 4 A and 4B isoforms), H-Ras, N-Ras. Subsequently, separated proteins were transferred onto a nitrocellulose blotting membrane 0.2 μm by using a TransBlot turbo Transfer System (Bio-Rad). The blots were probed as indicated in the figures with the antibodies diluted as described in the Key Resources Table. The membranes were washed 3 times with PBST (0.2% (v/v) Tween 20 in PBS) and then incubated with anti-mouse or anti-rabbit IRDye800CW or IRDye680RD/LT conjugated secondary antibodies. Finally, protein bands were detected using a LI-COR ODYSSEY CLx system. Band intensities were quantified using Fiji and normalized to GAPDH. The relative abundances of phosphorylated ERK1/2 and phospho-Akt were quantified as the ratios of the intensities of phosphorylated proteins and the total proteins.

2.12. Quantitative RT-PCR of gene transcripts

Cells were seeded at a density of 100,000 cells/ mL of a 6-well plate and transfected with siRNAs directed against *KRAS*, *NRAS* and *HRAS*. Note that the *HRAS* siRNA against the human mRNA was also targeting the identical sequence of the mouse mRNA.

After culturing in low serum medium, cells were collected as indicated in the figures. Total RNA was isolated using Trizol according to the manufacturer's protocol. Reverse transcription was performed with 1 μg of total RNA using SuperScriptIII Reverse Transcriptase. The relative abundance of *KRAS*, *NRAS* and *HRAS*, gene transcripts was analyzed by using SsoAdvanced Universal SYBR Green Supermix on the CFX-connect real-time PCR instrument (Bio-Rad) and Bio-Rad CFX Manager Software. Specific amplicons were detected for *KRAS* (both K-Ras4A and K-Ras4B splice variants), *NRAS, HRAS*, and *GAPDH*. Forward and reverse primer sequences of *KRAS* amplicons were described previously (Tsai et al., 2015). Primers for amplification of *NRAS, HRAS* and *GAPDH* amplicons were based on primers from Origene or designed using the online tool 'OligoPerfect Primer Designer'. The mRNA sequences of mouse *HRAS* (NM_008284.3) and *GAPDH* (NM_008084.4) were used as templates for primer design. The relative mRNA expression level was calculated using the $2^{-\Delta\Delta Ct}$ method by normalizing to *GAPDH* expression (Livak and Schmittgen, 2001).

2.13. Data and statistical analysis

Prism 9 (GraphPad) was used for the preparation of plots, heatmaps, data and statistical analysis. Data represent means of 3 or more independent biological repeats (N). Each biological repeat consisted of at least 2000 cells. Marker positive/ negative cell fractions, p, were logit transformed, according to logit(p)=ln(p/1-p), to obtain continuous values for statistical comparison. Comparison of means was then performed using one-way ANOVA, unless otherwise mentioned in the figure legends. Bar plots show mean ± SEM. Sample means were compared with the chemical-, wild type- or time 0 d- control sample, unless otherwise indicated using horizontal lines. Statistical significance was represented as follows: * $p < 0.05$; ** $p < 0.01$; *** $p < 0.001$; **** $p < 0.0001$ above the respective bar plot.

3. Results

3.1. Benchmarking of flow cytometry-based analysis of C2C12 differentiation

Differentiation stage-specific markers of mouse muscle C2C12 cells correlate with those identified during muscle development *in vivo* (Fig. 1**A**) (Yin et al., 2013). Both the MAPK- and PI3K-pathways downstream of Ras are characteristically regulated during differentiation (Bennett and Tonks, 1997; Wakioka et al., 2001; Xu and Wu, 2000). The C2C12 model therefore offers the opportunity to study the impact of Ras-pathway disease variants and targeted drug treatments on cellular differentiation.

We first benchmarked this assay against conventional phenotypic and immunoblotting-based differentiation analysis. C2C12 cell myoblasts assume a roundish-rhomboid morphology when cultured in high serum (day 0) (Fig. 1**B**). Medium switching to low serum induces differentiation (day 1), which alters the morphology of cells to become increasingly more spindle shaped. From day 2 to day 3 after serum switching the number of spindle shaped cells visibly increased, and further elongation with subsequent fusion resulted in a robust myotube assembly at day 5 (Fig. 1**B**). While determining the fraction of nuclei incorporated into myotubes can measure the overall progression of differentiation as the fusion index, this and related methods are quite tedious and allow only for the analysis of small cell numbers (Velica and Bunce, 2011).

In addition, muscle progenitor and differentiation markers are commonly analyzed using immunoblotting, which however captures only the averaged response across the heterogenous, differentiating cell pool. This became obvious when we compared immunoblotting- and flow cytometry-derived results of various muscle differentiation markers during the 5-day differentiation period. Immunoblotting revealed a nearly constant Pax7 protein expression (Fig. 1**C**), which was matched by an almost constant mean Pax7 intensity in the flow cytometry-based analysis (Fig. 1**D**). However, the fraction of Pax7 positive (Pax7+) cells increased from day three onwards (Fig. 1**D**). By contrast, analysis of the early differentiation marker myogenin by immunoblotting suggested a linear increase of the muscle-specific transcription factor during differentiation (Fig. 1**E**). This increase is however not due to an increased number of myogenin positive cells, but an increased mean expression level of the transcription factor in the population, as revealed by the flow cytometry data (Fig. 1**F**). Both immunoblotting (Fig. 1**G**) and flow cytometric analysis (Fig. 1**H**) confirmed that the expression of the late differentiation marker myosin heavy chain (MyHC) rapidly increased between days 2 and 3. In this case both the fraction of MyHC+ cells and the mean expression level in the population increased (Fig. 1**H**). The flow cytometry-based analysis of C2C12 cell differentiation therefore resolves population level differences in the expression of differentiation markers that may remain hidden in other common types of differentiation analyses. We therefore recently established a protocol to measure C2C12 cell differentiation using the flow cytometric quantification of the MyHC+ fraction, which we furthermore automated by our custom R-script software FlowFate (Parisi et al., 2023).

The sensitivity of this assay furthermore enabled us to detect an apparent decline in the differentiation potential with an increase in passage number. Cells with the passage number six (Fig. 1**H**) arrived at ~20% MyHC+ cells at day 3, while this fraction declined to ~15% in passage eight and slightly further to ~13% in passage ten (Fig. S1A**-D**). At the same time, the number of differentiated cells at day 0 in high serum increased in the same order, suggesting that a leakage into differentiation occurs due to passaging even in high serum. As this reduced the net change of the fraction of differentiated cells, i.e. the dynamic range of this assay, we aimed at employing cells with passage numbers from six to nine and included internal references wherever possible. Nevertheless, a residual background fluctuation inherent to variations caused by the passage numbers can be observed in our data that were composed from independent biological repeats across a longer time span.

3.2. Differentiated cells arise from the major pool of Pax7-/ MyHC- transit amplifying cells

Our analysis revealed that the muscle progenitor marker Pax7 is expressed by a minor sub-population of C2C12 cells (1–2%) before and after induction of differentiation (Fig. 1**D**). It is therefore impossible that this population of myoblasts provides the bulk of differentiated Pax7-/ MyHC+ myotubes. Instead, double labelling revealed that concomitant with the increase of the Pax7-/ MyHC+ differentiated cells, a Pax7-/

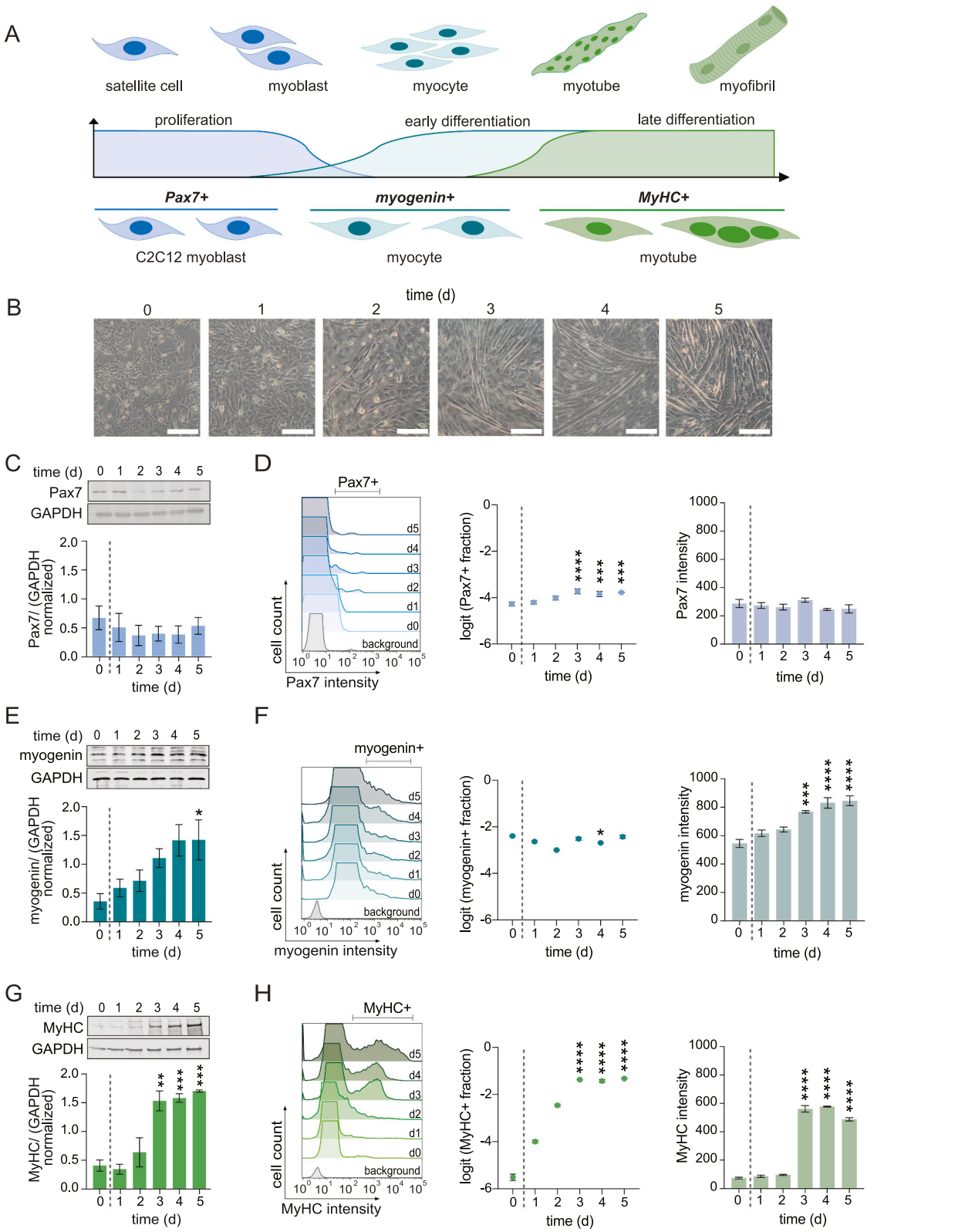

Fig. 1. Improved characterization of C2C12 cell differentiation by flow cytometry. (**A**) Differentiation of skeletal muscle *in vivo* (top) and of C2C12 cells (bottom) are similar based on marker expression. (**B**) C2C12 cells were differentiated by switching to low serum medium for indicated times. Brightfield images were obtained at 10 × magnification. Scale bars, 200 μm. (**C-H**) Representative immunoblots and quantification of Pax7 (C), myogenin (E) and MyHC (G) expression in C2C12 cells; N = 3, passage number 6. Representative flow cytometry histograms of marker+ cells at indicated times after serum switch (left). Quantification of logit transformed marker+ fractions (middle) and geometric means of intensities (right). Analyzed markers were Pax7 (D), myogenin (F) and MyHC (H); N = 3, passage number 6. The switch to low serum medium for differentiation is here and subsequently indicated with a vertical dashed line.

MyHC- subpopulation decreased that constitutes the bulk of the C2C12 cell line (Fig. 2**A**). This strongly suggests that the MyHC+ differentiated cells arise from the Pax7-/ MyHC- cells.

To understand how this large pool of Pax7-/ MyHC- cells is maintained under high serum conditions, we analyzed the proliferation of the Pax7+ and Pax7- populations by co-labelling Ser10-phosphorylated histone H3 (pH3), a marker of mitotic and proliferative activity (Goto et al., 1999). While ~23% of Pax7+ myoblasts were also pH3+ at day 0 in high serum, only ~4% of Pax7- cells were pH3+, suggesting that these latter cells have a much lower mitotic activity. After switching to low serum, the fraction of mitotically active Pax7+ cells dropped slightly, consistent with persistent mitotic activity in the Pax7+ fraction

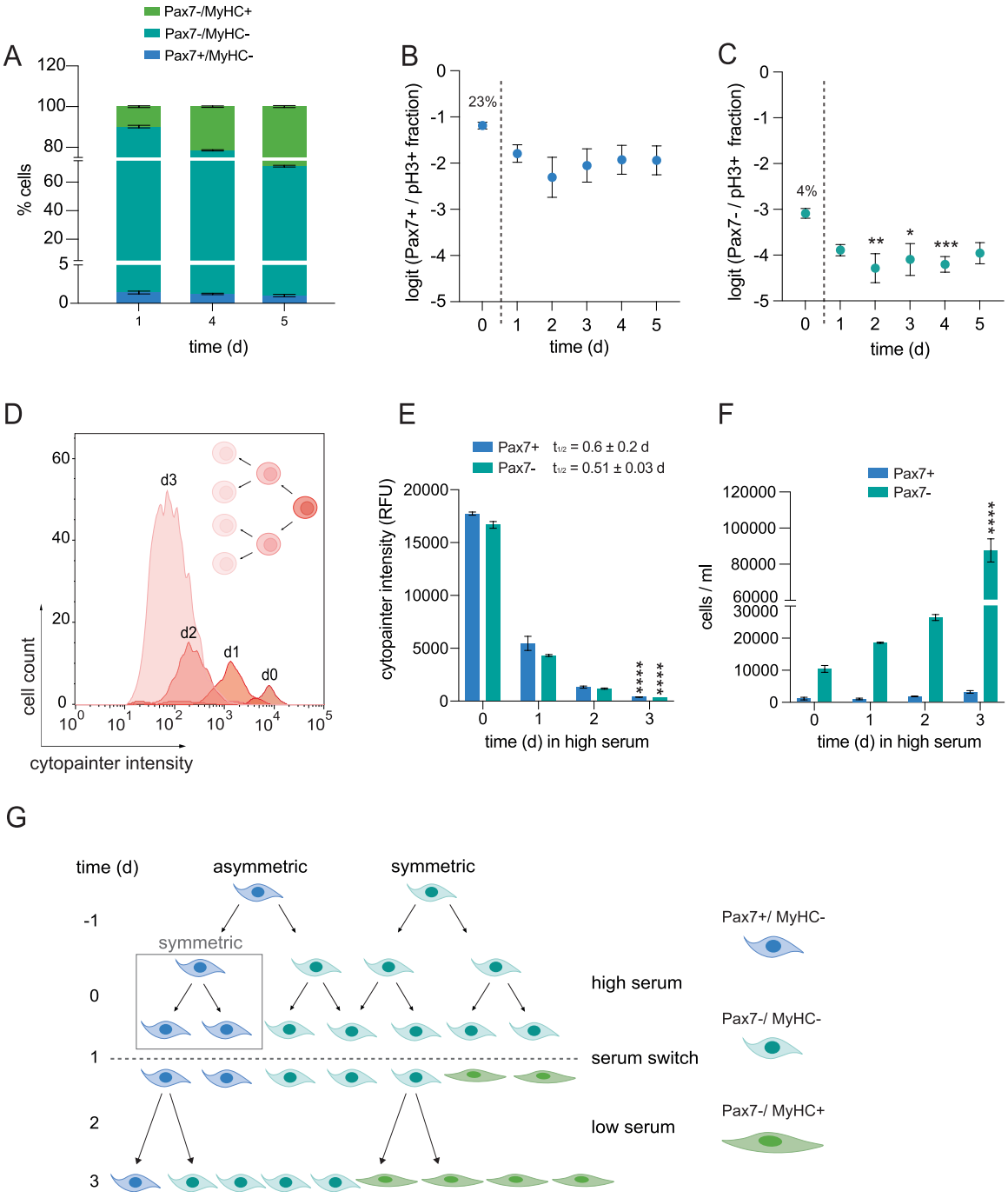

Fig. 2. A major pool of Pax7-/ MyHC- transit amplifying cells gives rise to Pax7-/ MyHC+ differentiated cells. (**A**) Flow cytometric analysis of C2C12 cell subpopulations after indicated times of differentiation; N ≥ 2, passage number 8–9. (**B,C**) Quantification of mitotically active (pH3+) Pax7+ (B) and Pax7- (C) subpopulations; N = 6, passage number 7–8. (**D**) Representative histograms of cytopainter dye dilution experiments from C2C12 cells proliferating in high serum medium for indicated times. Inset schematic illustrates dye dilution upon cell division. (**E**) Quantification of dye dilution experiments as in (D). Geometric means of fluorescence intensities of cytopainter deep red-labelled Pax7+ and Pax7- cells; N = 3, passage number 7–8. Half-life ($t_{1/2}$) of each fluorescence decay was calculated as described in methods. (**F**) Analysis of cell concentrations of Pax7+ and Pax7- populations proliferating in high serum; N = 3, passage number 7–8. (**G**) Revised population model for C2C12 cells. Our data suggest that Pax7+/ MyHC- progenitors divide to some extent symmetrically (boxed), but mostly asymmetrically, to self-renew and expand the number of slowly proliferating Pax7-/ MyHC- transit amplifying cells. This major pool of cells can be triggered to partially differentiate into Pax7-/ MyHC+ cells in low serum.

(Fig. 2**B**). The pH3+ mitotic fraction in the Pax7- population however decreased significantly upon serum switching, in agreement with cells becoming post-mitotic upon differentiation (Fig. 2**C**).

The higher proliferation rate of Pax7+ cells in high serum was further supported by dye-dilution experiments. The non-toxic cytopainter dye is diluted ~2-fold during each cell division, which was reflected by the decrease in the geometric means of fluorescence intensities in an exponentially growing cell population (Fig. 2**D,E**). When cultured under high serum, the cytopainter labelling decayed at a comparable rate in both Pax7+ and Pax7- subpopulations (Fig. 2**E**). At the same time, the number of Pax7- cells increased exponentially during the 3-day culture in high serum, while that of Pax7+ cells only marginally increased (Fig. 2**F**).

This proliferation pattern is reminiscent of other developmental systems where a minor pool of progenitors asymmetrically divides to generate one progenitor and one transit amplifying cell. The latter then expand exponentially, while the progenitor pool is preserved (Chia et al., 2008). This setup is not only critical during development but also for tissue homeostasis and regeneration in the adult (Gomez-Lopez et al., 2014; Post and Clevers, 2019).

Our data therefore suggest that under high serum conditions, the Pax7-/ MyHC- transit amplifying cells are replenished via predominantly asymmetric cell divisions of the highly proliferative Pax7+/ MyHC- progenitors, which explains the similar half-life of Pax7+ and Pax7- cell dye dilutions (Fig. 2**E,G**). The Pax7-/ MyHC- cells divide slower and likely symmetrically and furthermore continue to be replenished by the asymmetrically dividing progenitors, which explains the exponential expansion of Pax7- cells (Fig. 2**F,G**). With terminal differentiation, the Pax7- pool becomes post-mitotic and gradually forms myocytes and myotubes while expressing MyHC (Fig. 2**C,G**).

3.2.1. *K-Ras depletion increases, while H-Ras depletion decreases differentiation*

It was previously suggested that the three cancer associated Ras genes, *KRAS*, *NRAS* and *HRAS* all promote muscle differentiation via the PI3K-pathway (Lee et al., 2010). However, the individual contributions of the Ras genes on the above established three subpopulations of C2C12 cells is unknown. We therefore utilized siRNA-mediated knockdown to specifically downmodulate endogenous *RAS* isoforms and analyzed the effect on the Pax+/ MyHC- progenitors, Pax7-/ MyHC- transit amplifying cells and Pax7-/ MyHC+ terminally differentiated cells during differentiation.

Ras isoform specificity of knockdowns was validated by both immunoblotting (Fig. S2) and quantitative RT-PCR (Fig. S3). This analysis surprisingly revealed that knockdown of *NRAS* significantly increased K-Ras4A/B and H-Ras protein expression levels on day 1 (Fig. S2F), which was for K-Ras4A/B also reflected on the mRNA-level (Fig. S3D). Hence, this effect is likely not an unspecific siRNA activity, but an endogenous feedback mechanism. In addition, *NRAS* knockdown also downmodulated H-Ras mRNA on day 4 (Fig. S3D). Otherwise, all knockdowns remained isoform specific with an average knockdown efficiency of $\geq$ 35% on the protein level during the 5-day differentiation period (Fig. S2C**,E,G**).

While the specific knockdown of *KRAS* (i.e., of both K-Ras4A and K-Ras4B proteins) led only to a slight reduction of progenitors (Fig. 3**A**), a significant drop in the fraction of transit amplifying cells was noticeable (Fig. 3**B**). Importantly, the population of differentiated cells was significantly increased upon *KRAS* knockdown (Fig. 3**C**). By contrast no significant effects were observed with the *NRAS* knockdown (Fig. 3**D-F**). However, it is plausible to assume that any effect due to the *NRAS* knockdown is compensated by the induced upregulation of K-Ras and H-Ras (Fig. S2F). A markedly different outcome was observed upon knockdown of *HRAS*, which did not alter the progenitor fraction (Fig. 3**G**) but significantly increased the fraction of transit amplifying cells (Fig. 3**H**), which then resulted in a significantly decreased fraction of differentiated cells (Fig. 3**I**).

These population changes are accompanied by a drop in MAPK- and mTORC2-signalling, potentially in an isoform specific manner (Fig. S4). We observed a decrease of relative Thr202/Tyr204-phosphorylated ERK 1/2 (pERK) levels upon *KRAS* or *HRAS* knockdowns (Fig. S4A**,B,D**), but essentially no change in the case of *NRAS* knockdown (Fig. S4C). It can thus be speculated, that MAPK-signaling is relevant for both progenitor maintenance by K-Ras4A/B (Fig. 3**A**) and expansion of differentiated cells by H-Ras (Fig. 3**I**). By contrast, downregulation of any *RAS* isoform strongly reduced relative Ser473-phosphorylated Akt1 (pAkt) downstream of Ras and mTORC2 (Kovalski et al., 2019), with the strongest effect for *HRAS* knockdown (Fig. S4E**-H**).

Taken together, we postulate distinct roles for the three Ras isoforms in regulating C2C12 differentiation (Fig. 3**J**). K-Ras4A/B proteins seem important to maintain the Pax7+ progenitor pool and prevent differentiation of the transit amplifying cells, while H-Ras seems to facilitate this (Fig. 3**A-C**). N-Ras may have a similar and therefore partially redundant role, which may however be obscured given that its downregulation unexpectedly upregulates K-Ras and to a lesser extent H-Ras (Fig. 3**D-F**). This may correspond to a fail-safe mechanism, which makes sense in the context that *NRAS* is the evolutionary more recent Ras gene (Garcia-Espana and Philips, 2023).

3.3. *Oncogenic K-RasG12V blocks differentiation of transit amplifying cells*

It is well established that overactive MAPK-activity, such as associated with disease variants of pathway genes, blocks C2C12 cell differentiation (Konieczny et al., 1989; Wakioka et al., 2001). However, it is unknown, in which subpopulation these defects manifest and whether proliferation is increased, as typically assumed for oncogenic Ras-transformed cells.

Both oncogenic mutations as well as overexpression of Ras proteins is found in many cancers. Our flow cytometry-based differentiation assay offers the opportunity to exactly quantitate the expression level-dependent effect of both insults on differentiation, by gating for distinct transient expression levels of mEGFP-tagged wild-type or oncogenic K-Ras4B (hereafter K-Ras). Typically, 2000 – 3000 transfected cells were analyzed per condition, a number that remained constant until day 2 of differentiation, when expression started to drop (Fig. S5A**,B**). This transient perturbation of differentiation is necessary, as in stable transfectants the homeostasis of the mixed C2C12 cell pool would be permanently disrupted. For both constructs, most cells expressed in an expression window, which we defined as up to 10-fold above auto-fluorescence background of untransfected cells (Fig. S5C**, D**). A high-expression window essentially comprised all cells with expression levels beyond the former threshold.

In C2C12 cells expressing wt K-Ras in the low window, the fraction of Pax7+/ MyHC- progenitors remained essentially constant (Fig. 4**A**). As observed for untransfected C2C12 cells (Fig. 2**A**), a decrease in the pool of transit amplifying Pax7-/ MyHC- cells (Fig. 4**B**) was matched by an increase in the number of differentiated Pax7-/ MyHC+ cells over the 5 day differentiation period (Fig. 4**C**). In cells expressing wt K-Ras in the high window, the fraction of progenitor cells appeared unaltered (Fig. 4**A**). High wt K-Ras expression then resulted in a significantly decreased fraction of transit amplifying cells on days 4 and 5 as compared to the low-expression window (Fig. 4**B**), which was matched by a significantly increased fraction of differentiated cells on these days (Fig. 4**C**).

The fraction of progenitors appeared likewise unaltered in the GFP low and high windows of cells expressing K-RasG12V (Fig. 4**D**). However, the fraction of transformed transit amplifying cells showed a smaller decrease as compared to their wt K-Ras counterparts (Fig. 4**E**), irrespective of the expression level. This was matched by a reduced increase of differentiated cells, notably in the high-expression window (Fig. 4**F**).

It is generally assumed that oncogenic Ras mutants increase

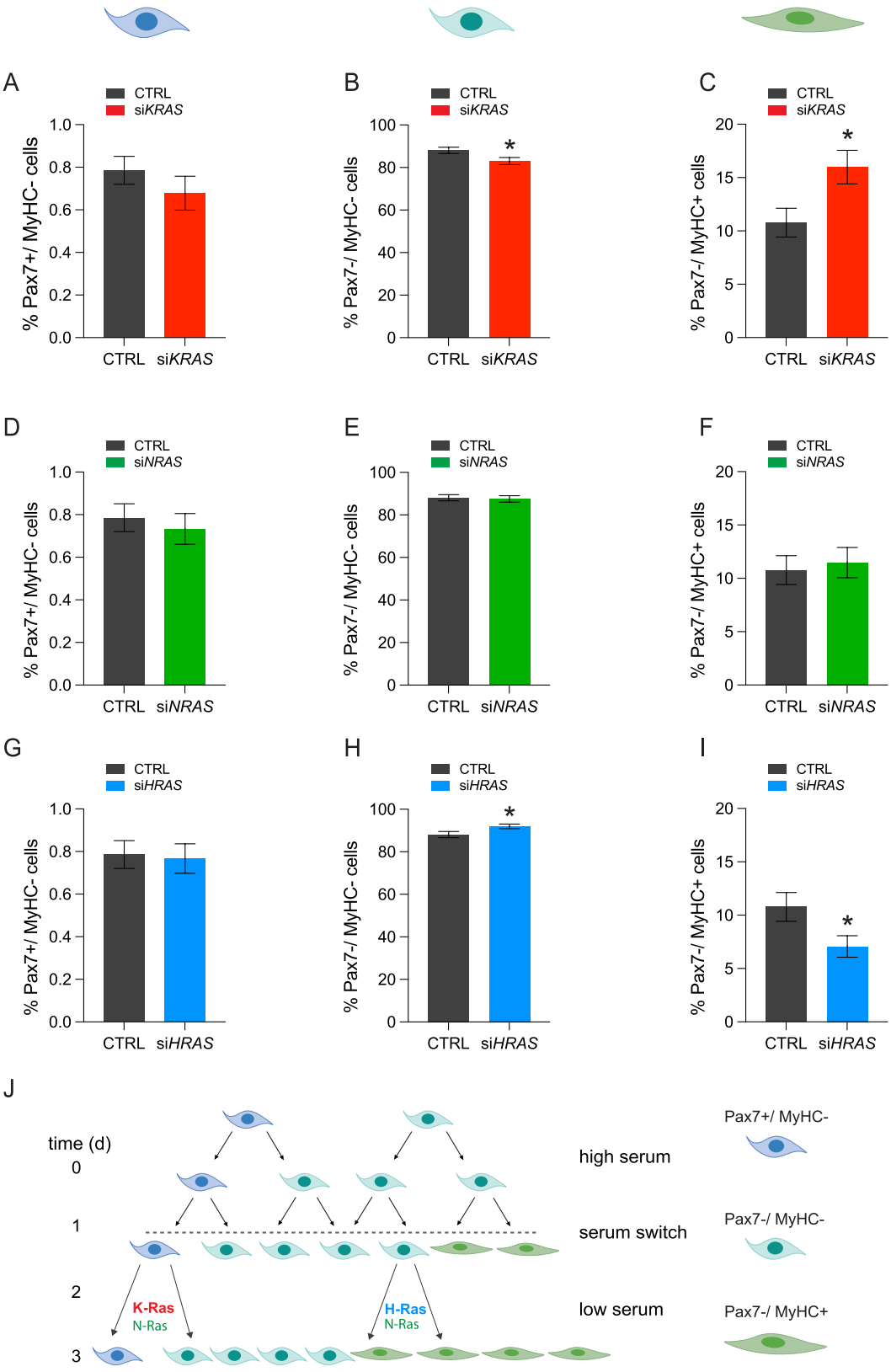

Fig. 3. K-Ras4A/B blocks whereas H-Ras promotes C2C12 differentiation. (**A-I**) Flow cytometric quantification of double-labelled C2C12 cells. At day 0 cells were treated with si*KRAS* to knock down both isoforms K-Ras4A/B or control siRNA (CTRL) (A-C). Analogous treatments were done using si*NRAS* (D-F) or si*HRAS* (G-I). Then the fractions of Pax7+/ MyHC- progenitors (A,D,G), Pax7-/ MyHC- transit amplifying cells (B,E,H) and Pax7-/ MyHC+ differentiated cells (C,F,I) were determined by flow cytometric analysis with daily sampling between day 1 and 5. Ideograms of cells at the top indicate the analyzed cell population in the column of panels; N ≥ 4, passage number 6–7. Statistical significance was calculated using the unpaired t-test. (**J**) Update of our population model for C2C12 cell differentiation with proposed participation of Ras isoforms in differentiating cell divisions.

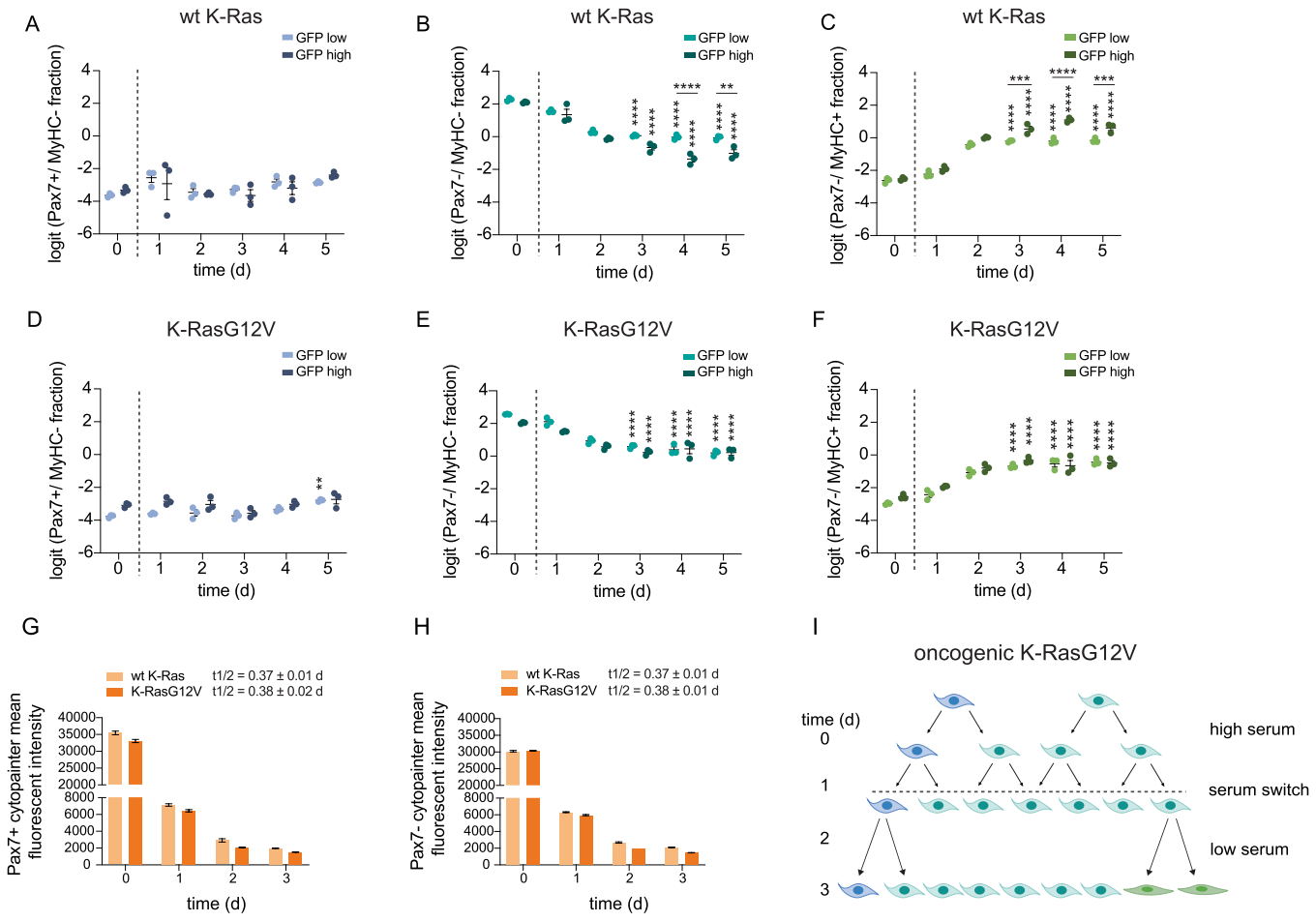

Fig. 4. Oncogenic K-Ras4B blocks differentiation of transit amplifying cells. (**A-C**) Flow cytometric analysis of temporal evolution of Pax7+/ MyHC- progenitors (A), Pax7-/ MyHC- transit amplifying cells (B) and Pax7-/ MyHC+ differentiated cells (C) after transfection of C2C12 cells with mEGFP-tagged wt K-Ras on day 0. Cells in the GFP low and GFP high expression windows were analyzed; N = 3, passage number 6. (**D-F**) Flow cytometric analysis of temporal evolution of Pax7+/ MyHC- progenitors (D), Pax7-/ MyHC- transit amplifying cells (E) and Pax7-/ MyHC+ differentiated cells (F) after transfection of C2C12 cells with mEGFP-tagged oncogenic K-RasG12V on day 0. Cells in the GFP low and GFP high expression windows were analyzed; N = 3, passage number 6. (**G,H**) Geometric means of fluorescence intensities of cytopainter orange-labelled Pax7+ (G) and Pax7- (H) of mEGFP-wt K-Ras or mEGFP-K-RasG12V expressing C2C12 cells; N = 3, passage number 6. Half-life ($t_{1/2}$) of each fluorescence decay was calculated as described in methods. (**I**) Population model for C2C12 cells transformed with oncogenic K-RasG12V, which blocks differentiation at the level of Pax7-/ MyHC- transit amplifying cells.

proliferation, which could impact on the fractions of cells that are analyzed here. We therefore again performed dye-dilution experiments to determine the doubling times in the Pax7+ and Pax7- populations of cells transfected with mEGFP-tagged wt K-Ras and K-RasG12V. Importantly, no significant differences were observed between the cytopainter dye dilution decay half-life values of wt K-Ras and K-RasG12V expressing cells in both the Pax7+ population (Fig. 4**G**) and the Pax7- population (Fig. 4**H**). K-RasG12V therefore does not stimulate proliferation more than the wt counterpart. Instead, K-RasG12V inhibits terminal differentiation of the transit amplifying cells (Fig. 4**I**).

3.4. Oncogenic and RASopathy-associated K-Ras mutants vary in their abilities to block differentiation

We next analyzed the impact of various mutant Ras-alleles on C2C12 cell differentiation. Again, we transiently transfected cells with GFP-variant tagged Ras-constructs and examined them by flow-cytometry in the GFP low window. We focused our analysis on day 3 of differentiation, as it is the earliest time point where differentiation measured by the fraction of MyHC+ cells becomes significantly different ($p < 0.0001$) between wt and oncogenic K-Ras in the GFP low window (Fig. 4**C,F**). In addition to the most frequent K-Ras mutations (Hobbs et al., 2016), we also included N-RasG12V and H-RasG12V, which all exhibit altered biochemical properties (Table S2) (Hunter et al., 2015; Moore et al., 2020; Rabara et al., 2019).

While the Pax7+ progenitor pool appeared increased by some oncogenic Ras mutants (Fig. 5**A**), their ability to block differentiation was most distinct (Fig. 5**B**). Interestingly, N-RasG12V and H-RasG12V, like K-RasG12D, left the progenitor fraction unaltered (Fig. 5**A**), while significantly blocking differentiation similar to all other oncogenic K-Ras mutants (Fig. 5**B**).

Aberrant differentiation is also observed in developmental diseases called RASopathies, where Ras-pathway genes are mutated in the germline. Thus, every cell in the body would essentially experience malfunctioning Ras that could broadly impact on development. Consistently, all RASopathies are characterized by multi-organ abnormalities, including of the musculoskeletal system (Stevenson et al., 2012). With a few exceptions, *RAS* mutations that are found in RASopathies are different from the ones seen in cancer (Bustelo et al., 2018; Castel et al., 2020). RASopathy mutants typically display multiple biochemical abnormalities but increase Ras-MAPK-signaling less than oncogenic mutants (Table S3) (Cirstea et al., 2013; Gremer et al., 2011).

Interestingly, the progenitor fractions of K-Ras RASopathy mutant transformed cells were mostly decreased (Fig. 5**C**), with significant drops observed for Y71H, Q22E, V14I and G60R.

Given the very small differences, it is difficult to draw conclusions

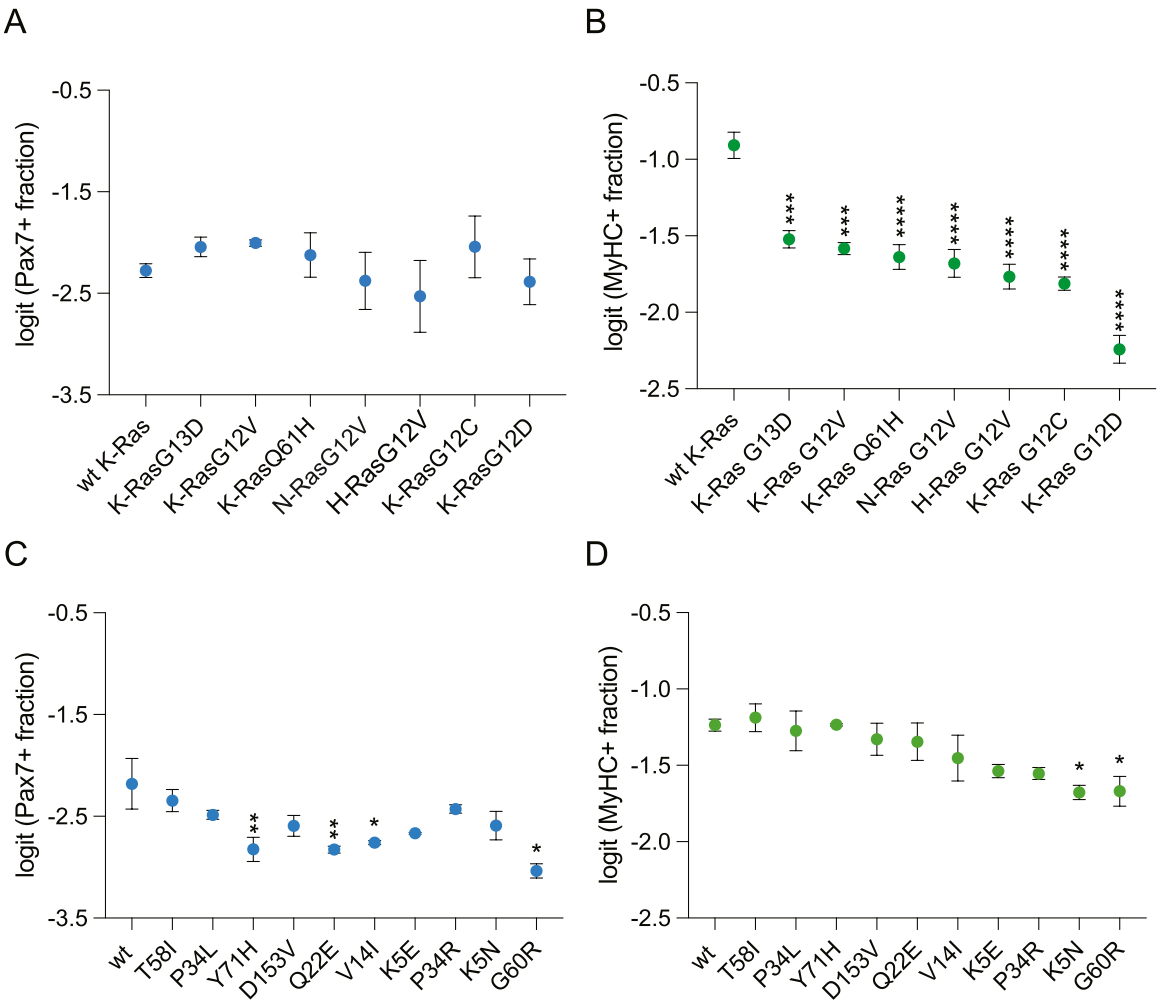

Fig. 5. All oncogenic Ras mutants block differentiation, while many RASopathy associated K-Ras mutants deplete progenitors. (**A,B**) EGFP-variant tagged oncogenic Ras constructs were transfected into C2C12 cells on day 0 and subsequently on day 3 of differentiation, Pax7+ cell fractions (A) and MyHC+ cell fractions (B) were analyzed by flow cytometry; N = 3, passage number 7. (**C,D**) EYFP-tagged K-Ras RASopathy mutants were transfected into C2C12 cells on day 0 and subsequently on day 3 of differentiation, Pax7+ cell fractions (A) and MyHC+ cell fractions (B) were analyzed by flow cytometry; N ≥ 2, passage number 9. In all plots, only cells in the GFP low expression windows were analyzed.

linking these observations to their biochemical features (Table S3). However, three of the four mutants have defective Raf-RBD binding as common phenotype, yet with the latter three being reported as mostly GTP-loaded (Table S3) (Cirstea et al., 2013; Gremer et al., 2011). They therefore combine loss- and gain-of-function features, which may have to be addressed quantitatively in cells to draw final conclusions.

Only two of the studied RASopathy mutants inhibited differentiation significantly (Fig. 5**D**). The strongest inhibition was seen with K-RasG60R, which however inhibited differentiation only as much as the weakest oncogenic mutant K-RasG13D. Together with the P34R mutant that also strongly inhibited differentiation, it shares reduced NF1-GAP sensitivity as a defect that is characteristic for all oncogenic mutants (Tables S2,**3**) (Gremer et al., 2011; Schubbert et al., 2006). Interestingly, the K5N mutant was described to have overall normal biochemical properties (Table S3), while it blocked differentiation as much as the G60R mutant. The underlying functional defect of the N-terminal mutant therefore remains to be elucidated.

Taken together with the results from the oncogenic mutants, these data are consistent with a significant role of the SPRED1/ NF1-complex and thus a potential requirement for the GDP-state of Ras to facilitate terminal differentiation of transit amplifying cells (Wakioka et al., 2001). Our data suggest that a disruption of differentiation steps, including the modulation of progenitor levels, may underpin Ras-driven oncogenesis and developmental aberrations.

3.4.1. K-RasG12C inhibitor profiling reveals their distinct ability to restore differentiation and induce toxic cell death

The past few years have seen the arrival of the first direct K-RasG12C inhibitors in the clinic (Punekar et al., 2022; Steffen et al., 2023). Classical cell-based assays profile these inhibitors based on their anti-proliferative and cell-killing activity. Here, we have the unique opportunity to quantify to what extent these inhibitors can restore inhibited differentiation that was induced by oncogenic K-Ras alleles.

First, we established that the employed DMSO concentrations below 0.1% that carried over from compound stocks do not impact on differentiation or have toxic effects (Fig. S6A,**B**). We then tested the two approved drugs sotorasib (AMG 510) and adagrasib (MRTX849) (Canon et al., 2019; Fell et al., 2020), as well as ARS-1620 the founder of current G12C-inhibitors (Janes et al., 2018), and MRTX1257, a close analogue of MRTX849 (Fell et al., 2020).

As just described, K-RasG12C decreased the fraction of MyHC+ cells more than K-RasG12V on day 3 (Fig. 6**A**). AMG 510 treatment at 3 μM did not have a restorative effect on differentiation of cells expressing wt K-Ras or K-RasG12V, however, it significantly increased the fraction of differentiated cells with K-RasG12C even beyond that of the wt-control (Fig. 6**A**). This was an interesting observation, as it may indicate a

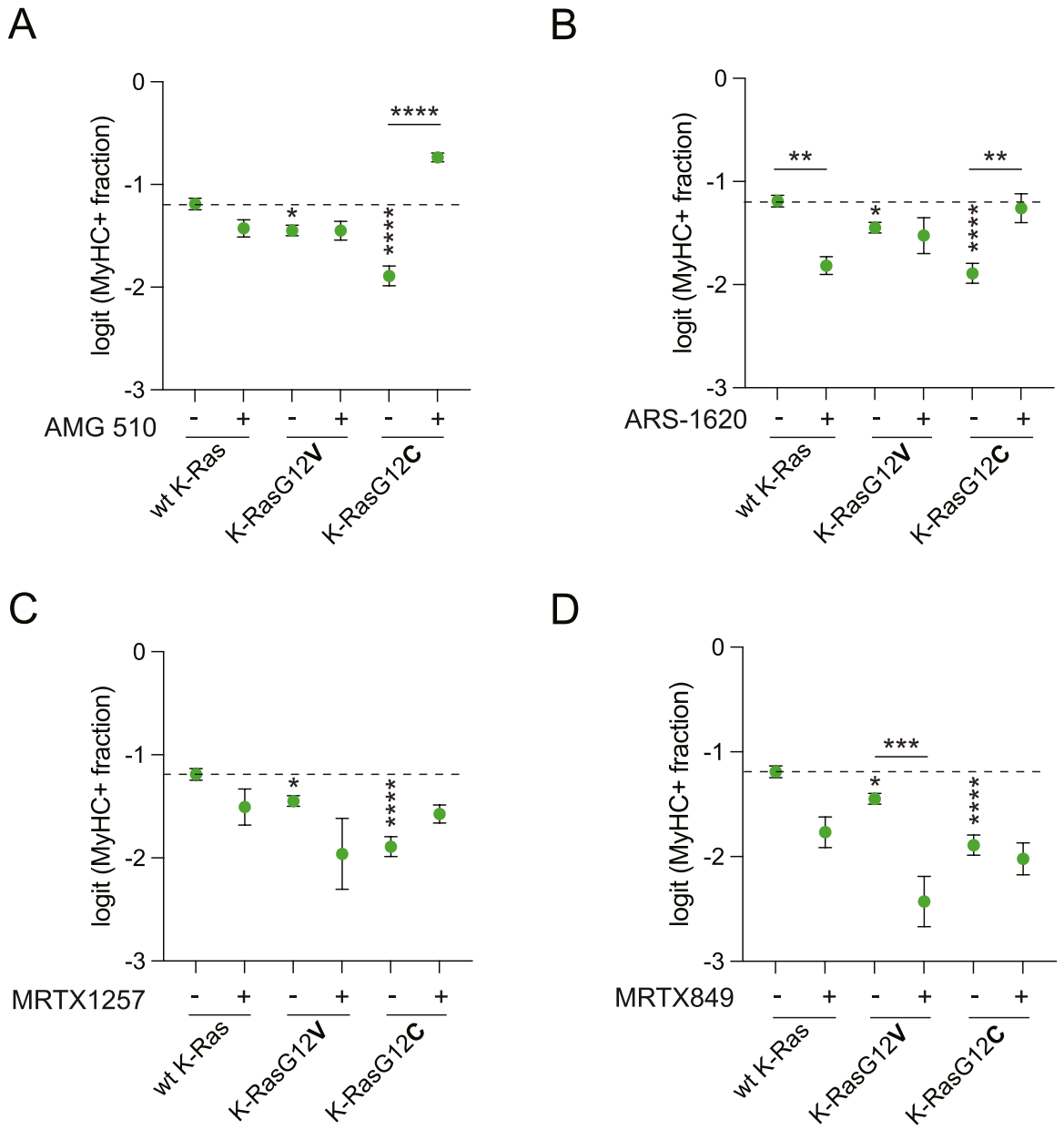

Fig. 6. K-RasG12C inhibitor profiling reveals their distinct abilities to restore differentiation. (**A-D**) Analysis of MyHC+ C2C12 cell fractions expressing GFP-variant tagged wt K-Ras, K-RasG12V and K-RasG12C on day 3 of differentiation. From day 1 onwards 3 μM of AMG 510 (A), ARS-1620 (B), MRTX1257 (C) or MRTX849 (D) or vehicle (DMSO 0.1% v/v) were added to cells; N = 4. In all plots, only cells from passage 9 in the GFP low expression windows were analyzed. Horizontal line marks the control value to facilitate comparison.

dominant negative action of AMG 510-bound K-RasG12C since this phenotype resembles that of the K-RasG12V-S17N with the S17N dominant negative mutation (Fig. S6C,**D**). This distinct ability of AMG 510 has not been reported previously. As expected, ARS-1620 could fully restore differentiation of K-RasG12C transformed C2C12 cells (Fig. 6**B**), while having no effect on the number of intact cells as also observed with AMG 510 (Fig. S6E,**F**).

By contrast, neither MRTX1257 nor MRTX849 could fully restore differentiation of K-RasG12C transformed C2C12 cells (Fig. 6**C,D**). Instead, we observed a reduction in the MyHC+ fraction in the drug treated K-RasG12V expressing cells (Fig. 6**C,D**). This was due to significant general toxicity of these compounds, which led to a significant drop of intact cells even for wt K-Ras expressing cells (Fig. S6G,**H**).

We more closely examined this K-RasG12C-inhibitor toxicity using 7-AAD-labelling, which indicates late apoptosis and necrosis in cells (Zembruski et al., 2012). This assay confirmed that under otherwise the same conditions the general toxicity increased in the order AMG 510 $\lesssim$ ARS-1620 $<$ MRTX1257 $\lesssim$ MRTX 849 in adherent and detached K-RasG12C transformed C2C12 cells (Fig. S6I,**J**).

This analysis demonstrates that both AMG 510 and ARS-1620 are effective and specific K-RasG12C inhibitors that can restore differentiation with no or little non-specific toxicity. On the other hand, both MRTX1257 and MRTX 849 display a broader toxicity, which undermines their differentiation restoring ability.

3.5. Profiling of clinical and pre-clinical RAS-MAPK-pathway inhibitors for their ability to restore differentiation

In extension of this analysis, we next assessed the oncogene- and allele-specific effect of targeted drugs on differentiation. Altogether we tested eight approved or clinically evaluated Ras-pathway inhibitors at 1 μM (except for trametinib at 0.1 μM and AMG 510 at 3 μM), which

target Ras trafficking (tipifarnib and cysmethynil), upstream activation (gefitinib, BI-3406), directly K-Ras (AMG 510, MRTX1133) and the major effector pathways downstream of Ras that are associated with cancer (trametinib, rapamycin).

Trafficking inhibitor tipifarnib, which inhibits farnesyltransferase, had a surprisingly broad effect on almost all K-Ras, N-Ras and H-Ras mutants to restore differentiation (Fig. 7**A**). By contrast, cysmethynil was essentially inefficacious (Fig. 7**A**), in agreement with its clinical performance (Lau et al., 2014).

The expected H-Ras specificity of tipifarnib treatment becomes more clearly visible, if we consider the net rescue effect of differentiation, i.e. the difference between the MyHC+ fraction with drug treatment and the DMSO-control (Fig. 7**B**). The second most sensitive allele was N-RasG12V, interestingly followed by K-RasG12V, while all other oncogenic K-Ras variants were less sensitive. This was surprising, given that K- and N-Ras can undergo their function-restoring alternative prenylation if farnesyltransferase is inhibited (Whyte et al., 1997).

Upstream inhibitors gefitinib, which blocks EGFR tyrosine kinase activity, only had a modest effect to restore differentiation of some K-Ras alleles (Fig. 7**A,B**), which essentially followed the order of the differentiation blocking activity of these K-Ras mutants (Fig. 5**B**). The SOS1 inhibitor BI-3406 performed better, leading to a substantial restoration, except for K-RasQ61H, which is known to have an elevated nucleotide exchange activity, while being impeded for activation by SOS1 (Gebregiworgis et al., 2021; Hofmann et al., 2021). By contrast, this compound was more efficient against K-RasG13D with a much-increased nucleotide exchange activity.

Next, AMG 510 showed the expected selectivity for K-RasG12C, with a minor effect on other alleles (K-RasG13D, K-RasG12V and N-RasG12V) (Fig. 7**A,B**). Allele selectivity, albeit not as clear as with AMG 510, was also seen with the low nanomolar non-covalent K-RasG12D-selective inhibitor MRTX1133 (Wang et al., 2022). Importantly, MRTX1133 restored differentiation to the highest levels observed so far for K-RasG12D but did appear to also mildly and non-specifically restore the differentiated fraction in other K-Ras alleles (Fig. 7**A,B**). These apparent non-specific effects of the two allele specific inhibitors may arise from non-covalent interactions with the switch II pocket of all K-Ras alleles. For compounds with the MRTX849 scaffold such non-specificity was explicitly demonstrated earlier (Vasta et al., 2022).

None of the former compounds though exerted an as strong pan-Ras effect as trametinib, which broadly restored differentiation across all alleles and isoforms (Fig. 7**A,B**). Only, drugs that have a known allele- or isoform-selectivity (tipifarnib for H-RasG12V, AMG 510 for K-RasG12C and MRTX1133 for K-RasG12D) matched or surpassed the effect of trametinib. This correlated with the clinical success of tipifarnib against H-RasG12V driven tumors and of AMG 510 against K-RasG12C driven tumors (Ho et al., 2021; Skoulidis et al., 2021). Finally, rapamycin broadly blocked differentiation, consistent with the importance of PI3K/mTORC1-signaling for myogenesis and terminal differentiation of C2C12 cells (Lee et al., 2010; Xu and Wu, 2000).

We, therefore, recapitulate closely the *in vivo* effects of targeted pharmacological agents. The broad effect of trametinib moreover highlights the central role of MAPK-activity to block differentiation. This becomes even clearer, when the net restoration of all oncogenic K-Ras alleles by trametinib is analyzed (Fig. 7**C**). One recovers a rank-order that anti-correlates with that of rapamycin (Fig. 7**D**) and correlates with the impact of these alleles on differentiation (Fig. 5**B**). This suggests that those K-Ras mutants that have a stronger dependence on MAPK-signaling, as expressed by their relative trametinib sensitivity (Fig. 7**C**), and lesser dependence on the PI3K/ mTORC1-signaling

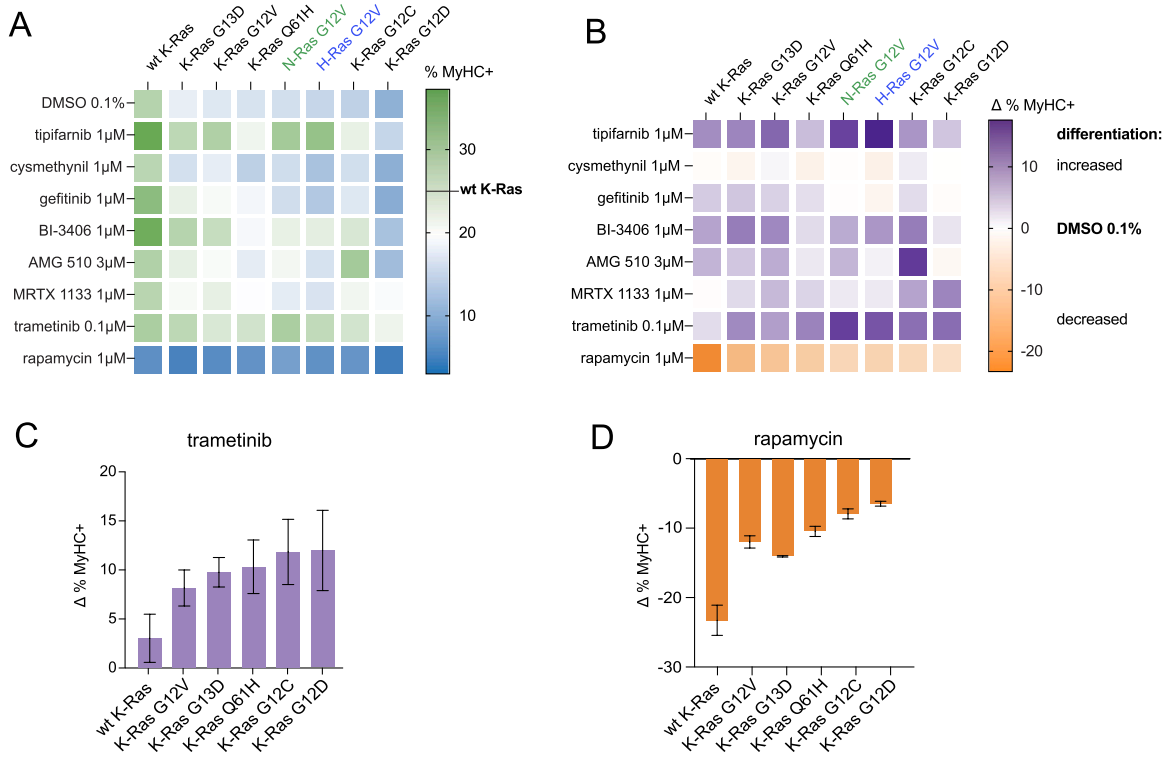

Fig. 7. Profiling of clinically tested Ras inhibitors for their ability to restore differentiation. (**A**) Heatmap showing % MyHC+ C2C12 cells, i.e. the absolute rescue effect, on day 3 of differentiation for each indicated condition. EGFP-variant tagged Ras-constructs were transfected on day 0; N = 3, passage number 7. The scale to the right shows the wt K-Ras differentiation level as a reference. Only cells in the GFP low expression windows were analyzed. (**B**) Net rescue effect of drugs. Plotted values were obtained by subtracting values from vehicle control (DMSO 0.1% v/v) treated samples in the top row from those treated with drugs in (A). The scale to the right shows the DMSO-control level as a reference. (**C**) Extract of data from (B). Rank-order of MAPK-pathway dependence of K-Ras variants judged by the trametinib induced net rescue. (**D**) Extract of data from (B). Rank-order of PI3K/ mTORC1-pathway dependence of K-Ras variants judged by the rapamycin induced net rescue.

(Fig. 7**D**), more profoundly block differentiation (Fig. 5**B**).

4. Discussion

The impact of RAS-MAPK-pathway disease mutants on cell transformation and the efficacy of novel Ras drug candidates are typically assessed in a small number of standard assays, such as NIH3T3 transformation and 2D/3D cancer cell proliferation assays, complemented by immunoblotting for markers of RAS-MAPK-pathway activity (Esposito et al., 2019). The impact on cell differentiation, though a known hallmark of cancer, has so far been vastly neglected (Chaffer and Weinberg, 2015; Hanahan, 2022).

Here we have established the C2C12 cell differentiation model to examine the effect of oncogenic Ras mutants and Ras-pathway drugs on differentiation. Importantly, this model recapitulates typical and fundamental steps of cell differentiation also found *in vivo* (Yin et al., 2013). Notably, the NF1 scaffold SPRED1 is upregulated upon differentiation, concomitant with a drop in MAPK-signaling, which allows to examine this core machinery of Ras-transformation in more detail (Stowe et al., 2012; Wakioka et al., 2001). This implies that our observations have broad implications not only for locally perturbed differentiation in cancer, but also for RASopathies, which are caused by aberrant Ras signaling throughout development. Our approach with a standard commercial cell line is advantageous as compared to the usage of human embryonic stem cells (hESC), which have also been used to identify compounds that maintain stemness or promote differentiation in more laborious, imaging-based high content screens (Barbaric et al., 2010; Desbordes et al., 2008; Jee et al., 2012; Sherman and Pyle, 2013).

Based on our analysis, we propose a new model of how in the C2C12 cell culture a small number of Pax7+ progenitor myoblasts are maintained, while the majority of cells is primed to differentiate. We suggest that frequent asymmetric divisions maintain the Pax7+/ MyHC- progenitor pool, while generating a transit amplifying Pax7-/ MyHC- pool of cells that exponentially expands within a few symmetric divisions. We furthermore provide evidence that the three cancer associated Ras genes, *KRAS*, *NRAS* and *HRAS* have a distinct, yet partially overlapping involvement in sustaining the proper trajectory from progenitors via here identified transit amplifying cells to differentiated cells. Individual Ras knockdowns generate distinct changes in the three populations that can hardly be explained by the alternative scenario where total Ras levels determine these alterations. Our data suggest a particular relevance of MAPK-signaling for K-Ras4A/B-dependent progenitor maintenance and H-Ras-dependent terminal differentiation. This is consistent with previous reports of MAPK inhibition resulting in increased differentiation (Rommel et al., 1999). While these data need further confirmation, our model adds another dimension to currently debated models for the isoform-specific functions of Ras, that include differences in plasma membrane organization and effector usage (Mo et al., 2018). The generally observed high expression level in particular of K-Ras4B in almost all tissues is consistent with its major function to sustain progenitors and being the evolutionary most ancient Ras isoform (Garcia-Espana and Philips, 2023; Hood et al., 2023).

It is well established that oncogenic Ras, constitutively active Raf or MEK1 inhibit myoblast differentiation (Dorman and Johnson, 1999; Olson et al., 1987; Weyman and Wolfman, 1998). However, we observed two distinct types of perturbed differentiation by Ras-pathway hyperactivation. The first is associated with overexpression of wt K-Ras that led to a more pronounced drop in the transit amplifying population matched by a significantly increased differentiation. By contrast, all NF1-GAP insensitive oncogenic Ras variants block terminal differentiation as compared to wt K-Ras. Moreover, those mutants that show a stronger sensitivity to trametinib and a lower sensitivity to rapamycin, are more potent to block differentiation. This order does not exactly fit with the mutation frequency of the oncogenic K-Ras alleles, but it could reflect their severity as expressed by the overall survival associated with the mutants. An exception is K-RasG13D, which is a biochemical outlier with a high nucleotide exchange rate, high intrinsic GTPase activity and NF1-GAP sensitivity (Hunter et al., 2015; Rabara et al., 2019).

As already inferred from their biochemical characterization, RASopathy associated K-Ras mutants are not or less able to block differentiation, consistent with these alterations being compatible with organismal development. Instead, it appears that many of them are defective in sustaining the C2C12 cell progenitor fraction. Intriguingly, the most potent RASopathy mutant K-RasG60R, which inhibits differentiation only as much as the weaker oncogenic K-Ras allele K-RasG13D, also displays a more prominent NF1-GAP resistance. The milder effects of RASopathy K-Ras mutants G60R and P34R can be explained by their decreased effector engagement, which also exists in a milder manifestation in the V14I mutant. We postulate that both K5-mutants somehow evade full-length NF1-GAP activity in the cell, given their ability to significantly block differentiation.

For all of the NF1-GAP resistant mutants, differentiation of transit amplifying cells is blocked, as shown in more detail for K-RasG12V. This is consistent with the fact that with the induction of differentiation, the potentially K-Ras-selective tumor suppressor complex of SPRED1 with the GAP NF1 can become active only after SPRED1-induction (Siljamaki and Abankwa, 2016; Stowe et al., 2012; Wakioka et al., 2001). Thus, MAPK-signaling would be sustained in transit amplifying cells, which prevents differentiation. This specifies that the oncogenic insult of hotspot-mutated Ras occurs at a defined point of the differentiation trajectory, an important fact that has not been recognized before. Moreover, this model implies molecular mechanistic and developmental commonalities between cancer and RASopathies, which have been long elusive (Castel et al., 2020).

In direct correlation with our muscle cell line observations, RASopathy patients display muscle weakness in particular in Costello syndrome (CS) (Stevenson et al., 2012; Stevenson and Yang, 2011). In the heterozygous *HRAS-G12V* CS mouse model a decreased muscle mass and strength was found, due to inhibited embryonic myogenesis and myofiber formation (Tidyman et al., 2022). This was due to an inhibited differentiation in the embryonic muscles, with a 23% increase in Pax7 expressing cells and a decrease in MyoD and myogenin expressing cells to 60–70% of the wt. A less severe skeletal myopathy is observed in the RASopathy cardiofaciocutaneous syndrome mouse model with a *BRAF-L597V* mutation (Maeda et al., 2021). Given the distinct penetrance of muscle phenotypes in RASopathies, one may assume this could be due to distinct mutant allele strengths, as suggested by our data. Alternatively, in muscle cells only certain alleles could become significant, while others would be tissue specifically contained, which is probably a less likely scenario. Importantly, these data corroborate the idea that the muscle phenotype in RASopathies is due to perturbed differentiation of stem/ progenitor cells, as has been observed in other muscle diseases notably in Duchenne muscular dystrophy, where asymmetric cell divisions of satellite cells are likewise not proceeding correctly (Feige et al., 2018).

Soft tissue rhabdomyosarcoma (RMS) of the muscle are frequently observed in RASopathies, such as Neurofibromatosis type 1, Noonan syndrome and CS (Skapek et al., 2019). RMS is the most common childhood soft-tissue sarcoma with only 30% survival in the metastatic disease. These tumors emerge from muscle progenitors/ myoblasts that failed to differentiate, albeit the exact cell of origin is still not well characterized (Skapek et al., 2019). Strikingly, this is exactly the phenotype we have observed in our data.

Two RMS subtypes are distinguished, the alveolar type in adolescents and the embryonal type in younger patients, which is associated with good prognosis, despite higher mutational burden (Shern et al., 2014). The former largely overlaps with the Pax-fusion positive molecular subtype, with neomorphic gain-of-function fusion proteins of Pax3 or Pax7 with FOXO1. In the Pax-fusion negative (embryonal) subtype of RMS, the Ras-pathway is activated by mutations in the pathway, while in the Pax-fusion positive subtype the upregulation of Ras pathway genes is found (Shern et al., 2014; Skapek et al., 2019). Interestingly, it is

one of the few cancer types where the three Ras isoforms are mutated at about equal frequency. Oncogenic Ras prevents differentiation in rhabdomyosarcoma (Yohe et al., 2018).

Finally, we profiled the effect of drugs on differentiation in a rapid and unique manner. Our assessment of four K-Ras-G12C inhibitors importantly demonstrates that inhibition of the oncogenic K-Ras also rescues differentiation. Yet, unexpected idiosyncrasies of these compounds were observed. Interestingly, the increase in differentiation that we observed with K-RasG12C bound AMG 510, may suggest a molecular complex that becomes dominant negative, similar to what is seen with the S17N-mutation. It is not likely that target-independent, off-target effects are responsible for this observation, as there is no effect with K-RasG12V expressing cells. By contrast, adagrasib (MRTX849) and more so MRTX1257 were less proficient in restoring differentiation, while inducing significantly more non-specific cell death. This is typically not desired, and in this particular case it may be attributed to the inhibition of wt K-Ras (Vasta et al., 2022). Their inhibition of other mutant *KRAS* alleles is probably beneficial in the clinical setting, where any anti-proliferative activity could be helpful and the activity against other *KRAS* alleles prevents their success if they evolved as a resistance mechanism (Liu et al., 2022).

Consistent with observations in the more complex hESC model and zebra fish larvae (Chen et al., 2011; Pal et al., 2012), we also noted the significant, dose-dependent effect of DMSO at concentrations above 0.2% on C2C12 cell differentiation and viability. Hence, our assay may be suitable to identify and explain differentiation perturbing, toxic effects of organic solvents or other substances that may correlate with their teratogenic potential.

We furthermore illustrate the enormous potential for Ras-pathway drug profiling on multiple Ras-disease mutants in our 8 × 8 matrix, which revealed a remarkable correlation of the ability of drugs to restore differentiation with their clinical efficacy in Ras disease treatment. Trametinib was very efficacious to restore differentiation of K-Ras mutants that profoundly blocked differentiation. Interestingly, the same order of sensitivity was found for tipifarnib, which may indicate that both drugs, tipifarnib and trametinib could work synergistically to restore differentiation. The broad capacity to restore differentiation by MEK-inhibition is paralleled by results obtained with myocyte cultures derived from the CS mouse model. Differentiation of those cells could be restored by the MEK inhibitor PD0325901, while the differentiation of the wt control was further increased. Importantly, this was mirrored by muscle-mass and -diameter increases *in vivo* to control levels (Tidyman et al., 2022). Thus, relative muscle strength development in RASopathy patients may also serve as a biomarker for treatment efficacy. We found that rapamycin was one of the few compounds, which prevented C2C12 cell differentiation. Others have previously shown that it inhibits differentiation that is promoted by the PI3K/ mTORC1- pathway (Hatfield et al., 2015). While the PI3K/ Akt/ mTORC1/ S6K1-axis is involved in hypertrophic muscle growth (Mounier et al., 2011; Yoon, 2017), the PI3K inhibitor GDC0941 led to muscle cell death in a CS mouse model and was deleterious *in vivo* (Tidyman et al., 2022). However, in the aging muscle, hyperactive mTORC1 appears to induce muscle damage and loss, hence low dose treatment with rapamycin analogue everolimus (RAD001) salvages this situation *in vivo* (Joseph et al., 2019). In the end, this compound analysis allowed us to estimate the utilization of the MAPK- and PI3K-pathway suggesting that oncogenic K-Ras alleles show a distinct dependence on these pathways. Interestingly, those mutants with a higher MAPK (trametinib)- and lower PI3K/ mTORC1 (rapamycin) -dependence were more potent to block differentiation.

Future developments of such drug-profiling derived models may enable us to predict efficacious drug combinations that do not only restore differentiation but in parallel also work in cancer therapy. The fact that we observe striking correlations of our differentiation data with overall Ras mutation strength and drug-responses observed in the clinic, suggests that we are looking here at a highly conserved function of Ras that is deeply engrained into the functioning of nearly every metazoan cell system. In order to devise therapies that can fully salvage the aberrant differentiation induced by Ras-pathway hyperactivation, we need to understand its impact on both cell proliferation and differentiation. The involvement of Ras beyond the G1-phase, where the Ras-MAPK-pathway is known to drive S-phase entry such as by stimulating cyclin D expression, is largely unknown. However, cell fate decisions are taken during M-phase, as stem/ progenitor cells symmetrically or asymmetrically divide. We therefore postulate a distinct role of Ras-pathway activity during this fundamental step, which cannot merely be explained by different strengths of the pathway output, but the underlying cell and developmental biology.

CRediT authorship contribution statement

Rohan Chippalkatti: Conceptualization, Formal analysis, Investigation, Methodology, Validation, Writing – original draft, Writing: review & editing. **Bianca Parisi:** Conceptualization, Formal analysis, Investigation, Methodology, Validation, Writing – original draft, Writing: review & editing. **Farah Kouzi:** Formal analysis, Investigation, Methodology. **Christina Laurini:** Formal analysis, Investigation, Methodology. **Nesrine Ben Fredj:** Formal analysis, Investigation, Methodology. **Daniel Kwaku Abankwa:** Conceptualization, Funding acquisition, Project administration, Supervision, Writing – original draft, Writing: review & editing.

Declaration of Competing Interest

The authors declare that they have no known competing financial interests or personal relationships that could have appeared to influence the work reported in this paper.

Data Availability

Data will be made available on request.

Acknowledgements

We thank Dr. Anthoula Gaigneaux for her invaluable advice on statistical analysis and Dr. Elisabeth Schaffner for proofreading the manuscript. This work was supported by funds provided by the University of Luxembourg and a grant from the Luxembourg National Research Fund (FNR) grant C19/BM/13673303-PolaRAS2 to D.K.A.

Appendix A. Supporting information

Supplementary data associated with this article can be found in the online version at doi:10.1016/j.ejcb.2024.151425.

References

Ahmadian, M.R., Stege, P., Scheffzek, K., Wittinghofer, A., 1997. Confirmation of the arginine-finger hypothesis for the GAP-stimulated GTP-hydrolysis reaction of Ras. Nat. Struct. Biol. 4, 686–689.

Altshuler, A., Verbuk, M., Bhattacharya, S., Abramovich, I., Haklai, R., Hanna, J.H., Kloog, Y., Gottlieb, E., Shalom-Feuerstein, R., 2018. RAS Regulates the Transition from Naive to Primed Pluripotent Stem Cells. Stem Cell Rep. 10, 1088–1101.

Ansieau, S., 2013. EMT in breast cancer stem cell generation. Cancer Lett. 338, 63–68.

Barbaric, I., Gokhale, P.J., Jones, M., Glen, A., Baker, D., Andrews, P.W., 2010. Novel regulators of stem cell fates identified by a multivariate phenotype screen of small compounds on human embryonic stem cell colonies. Stem Cell Res 5, 104–119.

Barretina, J., Caponigro, G., Stransky, N., Venkatesan, K., Margolin, A.A., Kim, S., Wilson, C.J., Lehar, J., Kryukov, G.V., Sonkin, D., Reddy, A., Liu, M., Murray, L., Berger, M.F., Monahan, J.E., Morais, P., Meltzer, J., Korejwa, A., Jane-Valbuena, J., Mapa, F.A., Thibault, J., Bric-Furlong, E., Raman, P., Shipway, A., Engels, I.H., Cheng, J., Yu, G.K., Yu, J., Aspesi Jr., P., de Silva, M., Jagtap, K., Jones, M.D., Wang, L., Hatton, C., Palescandolo, E., Gupta, S., Mahan, S., Sougnez, C., Onofrio, R. C., Liefeld, T., MacConaill, L., Winckler, W., Reich, M., Li, N., Mesirov, J.P., Gabriel, S.B., Getz, G., Ardlie, K., Chan, V., Myer, V.E., Weber, B.L., Porter, J., Warmuth, M., Finan, P., Harris, J.L., Meyerson, M., Golub, T.R., Morrissey, M.P., Sellers, W.R., Schlegel, R., Garraway, L.A., 2012. The Cancer Cell Line Encyclopedia enables predictive modelling of anticancer drug sensitivity. Nature 483, 603–607.

Batlle, E., Clevers, H., 2017. Cancer stem cells revisited. Nat. Med 23, 1124–1134.
Bennett, A.M., Tonks, N.K., 1997. Regulation of distinct stages of skeletal muscle differentiation by mitogen-activated protein kinases. Science 278, 1288–1291.
Brems, H., Pasmant, E., Van Minkelen, R., Wimmer, K., Upadhyaya, M., Legius, E., Messiaen, L., 2012. Review and update of SPRED1 mutations causing Legius syndrome. Hum. Mutat. 33, 1538–1546.
Brown, D.M., Parr, T., Brameld, J.M., 2012. Myosin heavy chain mRNA isoforms are expressed in two distinct cohorts during C2C12 myogenesis. J. Muscle Res Cell Motil. 32, 383–390.
Bustelo, X.R., Crespo, P., Fernandez-Pisonero, I., Rodriguez-Fdez, S., 2018. RAS GTPase-dependent pathways in developmental diseases: old guys, new lads, and current challenges. Curr. Opin. Cell Biol. 55, 42–51.
Canon, J., Rex, K., Saiki, A.Y., Mohr, C., Cooke, K., Bagal, D., Gaida, K., Holt, T., Knutson, C.G., Koppada, N., Lanman, B.A., Werner, J., Rapaport, A.S., San Miguel, T., Ortiz, R., Osgood, T., Sun, J.R., Zhu, X., McCarter, J.D., Volak, L.P., Houk, B.E., Fakih, M.G., O'Neil, B.H., Price, T.J., Falchook, G.S., Desai, J., Kuo, J., Govindan, R., Hong, D.S., Ouyang, W., Henary, H., Arvedson, T., Cee, V.J., Lipford, J.R., 2019. The clinical KRAS(G12C) inhibitor AMG 510 drives anti-tumour immunity. Nature 575, 217–223.
Castel, P., Rauen, K.A., McCormick, F., 2020. The duality of human oncoproteins: drivers of cancer and congenital disorders. Nat. Rev. Cancer 379, 1–15.
Chaffer, C.L., Weinberg, R.A., 2015. How does multistep tumorigenesis really proceed? Cancer Discov. 5, 22–24.
Chen, T.H., Wang, Y.H., Wu, Y.H., 2011. Developmental exposures to ethanol or dimethylsulfoxide at low concentrations alter locomotor activity in larval zebrafish: implications for behavioral toxicity bioassays. Aquat. Toxicol. 102, 162–166.
Chia, W., Somers, W.G., Wang, H., 2008. Drosophila neuroblast asymmetric divisions: cell cycle regulators, asymmetric protein localization, and tumorigenesis. J. Cell Biol. 180, 267–272.
Chippalkatti, R., Abankwa, D., 2021. Promotion of cancer cell stemness by Ras. Biochem Soc. Trans. 49, 467–476.
Cirstea, I.C., Gremer, L., Dvorsky, R., Zhang, S.C., Piekorz, R.P., Zenker, M., Ahmadian, M.R., 2013. Diverging gain-of-function mechanisms of two novel KRAS mutations associated with Noonan and cardio-facio-cutaneous syndromes. Hum. Mol. Genet 22, 262–270.
Crespo, P., Leon, J., 2000. Ras proteins in the control of the cell cycle and cell differentiation. Cell Mol. Life Sci. 57, 1613–1636.
de Alvaro, C., Martinez, N., Rojas, J.M., Lorenzo, M., 2005. Sprouty-2 overexpression in C2C12 cells confers myogenic differentiation properties in the presence of FGF2. Mol. Biol. Cell 16, 4454–4461.
Desbordes, S.C., Placantonakis, D.G., Ciro, A., Socci, N.D., Lee, G., Djaballah, H., Studer, L., 2008. High-throughput screening assay for the identification of compounds regulating self-renewal and differentiation in human embryonic stem cells. Cell Stem Cell 2, 602–612.
Dontu, G., Abdallah, W.M., Foley, J.M., Jackson, K.W., Clarke, M.F., Kawamura, M.J., Wicha, M.S., 2003. In vitro propagation and transcriptional profiling of human mammary stem/progenitor cells. Genes Dev. 17, 1253–1270.
Dorman, C.M., Johnson, S.E., 1999. Activated Raf inhibits avian myogenesis through a MAPK-dependent mechanism. Oncogene 18, 5167–5176.
Esposito, D., Stephen, A.G., Turbyville, T.J., Holderfield, M., 2019. New weapons to penetrate the armor: Novel reagents and assays developed at the NCI RAS Initiative to enable discovery of RAS therapeutics. Semin Cancer Biol. 54, 174–182.
Feige, P., Brun, C.E., Ritso, M., Rudnicki, M.A., 2018. Orienting Muscle Stem Cells for Regeneration in Homeostasis, Aging, and Disease. Cell Stem Cell 23, 653–664.
Fell, J.B., Fischer, J.P., Baer, B.R., Blake, J.F., Bouhana, K., Briere, D.M., Brown, K.D., Burgess, L.E., Burns, A.C., Burkard, M.R., Chiang, H., Chicarelli, M.J., Cook, A.W., Gaudino, J.J., Hallin, J., Hanson, L., Hartley, D.P., Hicken, E.J., Hingorani, G.P., Hinklin, R.J., Mejia, M.J., Olson, P., Otten, J.N., Rhodes, S.P., Rodriguez, M.E., Savechenkov, P., Smith, D.J., Sudhakar, N., Sullivan, F.X., Tang, T.P., Vigers, G.P., Wollenberg, L., Christensen, J.G., Marx, M.A., 2020. Identification of the Clinical Development Candidate MRTX849, a Covalent KRAS(G12C) Inhibitor for the Treatment of Cancer. J. Med Chem. 63, 6679–6693.
Garcia-Espana, A., Philips, M.R., 2023. Origin and Evolution of RAS Membrane Targeting. Oncogene 42, 1741–1750.
Gebregiworgis, T., Kano, Y., St-Germain, J., Radulovich, N., Udaskin, M.L., Mentes, A., Huang, R., Poon, B.P.K., He, W., Valencia-Sama, I., Robinson, C.M., Huestis, M., Miao, J., Yeh, J.J., Zhang, Z.Y., Irwin, M.S., Lee, J.E., Tsao, M.S., Raught, B., Marshall, C.B., Ohh, M., Ikura, M., 2021. The Q61H mutation decouples KRAS from upstream regulation and renders cancer cells resistant to SHP2 inhibitors. Nat. Commun. 12, 6274.
Golebiewska, A., Brons, N.H., Bjerkvig, R., Niclou, S.P., 2011. Critical appraisal of the side population assay in stem cell and cancer stem cell research. Cell Stem Cell 8, 136–147.
Gomez-Lopez, S., Lerner, R.G., Petritsch, C., 2014. Asymmetric cell division of stem and progenitor cells during homeostasis and cancer. Cell Mol. Life Sci. 71, 575–597.
Goto, H., Tomono, Y., Ajiro, K., Kosako, H., Fujita, M., Sakurai, M., Okawa, K., Iwamatsu, A., Okigaki, T., Takahashi, T., Inagaki, M., 1999. Identification of a novel phosphorylation site on histone H3 coupled with mitotic chromosome condensation. J. Biol. Chem. 274, 25543–25549.
Gremer, L., Merbitz-Zahradnik, T., Dvorsky, R., Cirstea, I.C., Kratz, C.P., Zenker, M., Wittinghofer, A., Ahmadian, M.R., 2011. Germline KRAS mutations cause aberrant biochemical and physical properties leading to developmental disorders. Hum. Mutat. 32, 33–43.
Gross, A.M., Frone, M., Gripp, K.W., Gelb, B.D., Schoyer, L., Schill, L., Stronach, B., Biesecker, L.G., Esposito, D., Hernandez, E.R., Legius, E., Loh, M.L., Martin, S., Morrison, D.K., Rauen, K.A., Wolters, P.L., Zand, D., McCormick, F., Savage, S.A., Stewart, D.R., Widemann, B.C., Yohe, M.E., 2020. Advancing RAS/RASopathy therapies: An NCI-sponsored intramural and extramural collaboration for the study of RASopathies. Am. J. Med Genet A 182, 866–876.
Gupta, P.B., Onder, T.T., Jiang, G., Tao, K., Kuperwasser, C., Weinberg, R.A., Lander, E. S., 2009. Identification of selective inhibitors of cancer stem cells by high-throughput screening, 138, 645–659.
Haghighi, F., Dahlmann, J., Nakhaei-Rad, S., Lang, A., Kutschka, I., Zenker, M., Kensah, G., Piekorz, R.P., Ahmadian, M.R., 2018. bFGF-mediated pluripotency maintenance in human induced pluripotent stem cells is associated with NRAS-MAPK signaling. Cell Commun. Signal 16, 96.
Hanahan, D., 2022. Hallmarks of Cancer: New Dimensions. Cancer Discov. 12, 31–46.
Hatfield, I., Harvey, I., Yates, E.R., Redd, J.R., Reiter, L.T., Bridges, D., 2015. The role of TORC1 in muscle development in Drosophila. Sci. Rep. 5, 9676.
Ho, A.L., Brana, I., Haddad, R., Bauman, J., Bible, K., Oosting, S., Wong, D.J., Ahn, M.J., Boni, V., Even, C., Fayette, J., Flor, M.J., Harrington, K., Kim, S.B., Licitra, L., Nixon, I., Saba, N.F., Hackenberg, S., Specenier, P., Worden, F., Balsara, B., Leoni, M., Martell, B., Scholz, C., Gualberto, A., 2021. Tipifarnib in Head and Neck Squamous Cell Carcinoma With HRAS Mutations. J. Clin. Oncol. 39, 1856–1864.
Hobbs, G.A., Der, C.J., Rossman, K.L., 2016. RAS isoforms and mutations in cancer at a glance. J. Cell Sci. 129, 1287-1292.
Hofmann, M.H., Gmachl, M., Ramharter, J., Savarese, F., Gerlach, D., Marszalek, J.R., Sanderson, M.P., Kessler, D., Trapani, F., Arnhof, H., Rumpel, K., Botesteanu, D.A., Ettmayer, P., Gerstberger, T., Kofink, C., Wunberg, T., Zoephel, A., Fu, S.C., Teh, J.L., Bottcher, J., Pototschnig, N., Schachinger, F., Schipany, K., Lieb, S., Vellano, C.P., O'Connell, J.C., Mendes, R.L., Moll, J., Petronczki, M., Heffernan, T.P., Pearson, M., McConnell, D.B., Kraut, N., 2021. BI-3406, a Potent and Selective SOS1-KRAS Interaction Inhibitor, Is Effective in KRAS-Driven Cancers through Combined MEK Inhibition. Cancer Discov. 11, 142–157.
Hood, F.E., Sahraoui, Y.M., Jenkins, R.E., Prior, I.A., 2023. Ras protein abundance correlates with Ras isoform mutation patterns in cancer. Oncogene 42, 1224–1232.
Hunter, J.C., Manandhar, A., Carrasco, M.A., Gurbani, D., Gondi, S., Westover, K.D., 2015. Biochemical and Structural Analysis of Common Cancer-Associated KRAS Mutations. Mol. Cancer Res 13, 1325–1335.
Janes, M.R., Zhang, J., Li, L.S., Hansen, R., Peters, U., Guo, X., Chen, Y., Babbar, A., Firdaus, S.J., Darjania, L., Feng, J., Chen, J.H., Li, S., Li, S., Long, Y.O., Thach, C., Liu, Y., Zarieh, A., Ely, T., Kucharski, J.M., Kessler, L.V., Wu, T., Yu, K., Wang, Y., Yao, Y., Deng, X., Zarrinkar, P.P., Brehmer, D., Dhanak, D., Lorenzi, M.V., Hu-Lowe, D., Patricelli, M.P., Ren, P., Liu, Y., 2018. Targeting KRAS Mutant Cancers with a Covalent G12C-Specific Inhibitor. Cell 172, 578–589 e517.
Jee, J., Jeon, H., Hwang, D., Sommer, P., Park, Z., Cechetto, J., Dorval, T., 2012. High content screening for compounds that induce early stages of human embryonic stem cell differentiation. Comb. Chem. High. Throughput Screen 15, 656–665.
Jindal, G.A., Goyal, Y., Burdine, R.D., Rauen, K.A., Shvartsman, S.Y., 2015. RASopathies: unraveling mechanisms with animal models. Dis. Model Mech. 8, 769–782.
Joseph, G.A., Wang, S.X., Jacobs, C.E., Zhou, W., Kimble, G.C., Tse, H.W., Eash, J.K., Shavlakadze, T., Glass, D.J., 2019. Partial Inhibition of mTORC1 in Aged Rats Counteracts the Decline in Muscle Mass and Reverses Molecular Signaling Associated with Sarcopenia. Mol. Cell Biol. 39.
Konieczny, S.F., Drobes, B.L., Menke, S.L., Taparowsky, E.J., 1989. Inhibition of myogenic differentiation by the H-ras oncogene is associated with the down regulation of the MyoD1 gene. Oncogene 4, 473–481.
Kovalski, J.R., Bhaduri, A., Zehnder, A.M., Neela, P.H., Che, Y., Wozniak, G.G., Khavari, P.A., 2019. The Functional Proximal Proteome of Oncogenic Ras Includes mTORC2. Mol. Cell 73, 830–844 e812.
Laplante, M., Sabatini, D.M., 2013. Regulation of mTORC1 and its impact on gene expression at a glance. J. Cell Sci. 126, 1713-1719.
Lassar, A.B., Thayer, M.J., Overell, R.W., Weintraub, H., 1989. Transformation by activated ras or fos prevents myogenesis by inhibiting expression of MyoD1. Cell 58, 659–667.
Lau, H.Y., Ramanujulu, P.M., Guo, D., Yang, T., Wirawan, M., Casey, P.J., Go, M.L., Wang, M., 2014. An improved isoprenylcysteine carboxylmethyltransferase inhibitor induces cancer cell death and attenuates tumor growth in vivo. Cancer Biol. Ther. 15, 1280–1291.
Lee, J., Choi, K.J., Lim, M.J., Hong, F., Choi, T.G., Tak, E., Lee, S., Kim, Y.J., Chang, S.G., Cho, J.M., Ha, J., Kim, S.S., 2010. Proto-oncogenic H-Ras, K-Ras, and N-Ras are involved in muscle differentiation via phosphatidylinositol 3-kinase. Cell Res 20, 919–934.
Li, C., Vides, A., Kim, D., Xue, J.Y., Zhao, Y., Lito, P., 2021. The G protein signaling regulator RGS3 enhances the GTPase activity of KRAS. Science 374, 197–201.
Li, W., Ma, H., Zhang, J., Zhu, L., Wang, C., Yang, Y., 2017. Unraveling the roles of CD44/CD24 and ALDH1 as cancer stem cell markers in tumorigenesis and metastasis. Sci. Rep. 7, 13856.
Liu, J., Kang, R., Tang, D., 2022. The KRAS-G12C inhibitor: activity and resistance. Cancer Gene Ther. 29, 875–878.
Livak, K.J., Schmittgen, T.D., 2001. Analysis of relative gene expression data using real-time quantitative PCR and the 2(-Delta Delta C(T)) Method. Methods 25, 402–408.
Maeda, Y., Tidyman, W.E., Ander, B.P., Pritchard, C.A., Rauen, K.A., 2021. Ras/MAPK dysregulation in development causes a skeletal myopathy in an activating Braf (L597V) mouse model for cardio-facio-cutaneous syndrome. Dev. Dyn. 250, 1074–1095.
Mathews, L.A., Keller, J.M., Goodwin, B.L., Guha, R., Shinn, P., Mull, R., Thomas, C.J., de Kluyver, R.L., Sayers, T.J., Ferrer, M., 2012. A 1536-well quantitative high-throughput screen to identify compounds targeting cancer stem cells. J. Biomol. Screen 17, 1231–1242.
McDonald 3rd, E.R., de Weck, A., Schlabach, M.R., Billy, E., Mavrakis, K.J., Hoffman, G. R., Belur, D., Castelletti, D., Frias, E., Gampa, K., Golji, J., Kao, I., Li, L., Megel, P.,

Perkins, T.A., Ramadan, N., Ruddy, D.A., Silver, S.J., Sovath, S., Stump, M., Weber, O., Widmer, R., Yu, J., Yu, K., Yue, Y., Abramowski, D., Ackley, E., Barrett, R., Berger, J., Bernard, J.L., Billig, R., Brachmann, S.M., Buxton, F., Caothien, R., Caushi, J.X., Chung, F.S., Cortes-Cros, M., deBeaumont, R.S., Delaunay, C., Desplat, A., Duong, W., Dwoske, D.A., Eldridge, R.S., Farsidjani, A., Feng, F., Feng, J., Flemming, D., Forrester, W., Galli, G.G., Gao, Z., Gauter, F., Gibaja, V., Haas, K., Hattenberger, M., Hood, T., Hurov, K.E., Jagani, Z., Jenal, M., Johnson, J.A., Jones, M.D., Kapoor, A., Korn, J., Liu, J., Liu, Q., Liu, S., Liu, Y., Loo, A.T., Macchi, K.J., Martin, T., McAllister, G., Meyer, A., Molle, S., Pagliarini, R. A., Phadke, T., Repko, B., Schouwey, T., Shanahan, F., Shen, Q., Stamm, C., Stephan, C., Stucke, V.M., Tiedt, R., Varadarajan, M., Venkatesan, K., Vitari, A.C., Wallroth, M., Weiler, J., Zhang, J., Mickanin, C., Myer, V.E., Porter, J.A., Lai, A., Bitter, H., Lees, E., Keen, N., Kauffmann, A., Stegmeier, F., Hofmann, F., Schmelzle, T., Sellers, W.R., 2017. Project DRIVE: A Compendium of Cancer Dependencies and Synthetic Lethal Relationships Uncovered by Large-Scale, Deep RNAi Screening. Cell 170, 577–592 e510.

Mo, S.P., Coulson, J.M., Prior, I.A., 2018. RAS variant signalling. Biochem Soc. Trans. 46, 1325–1332.

Moore, A.R., Rosenberg, S.C., McCormick, F., Malek, S., 2020. RAS-targeted therapies: is the undruggable drugged? Nat. Rev. Drug Discov. 19, 533–552.

Morrison, S.J., Kimble, J., 2006. Asymmetric and symmetric stem-cell divisions in development and cancer. Nature 441, 1068–1074.

Mounier, R., Lantier, L., Leclerc, J., Sotiropoulos, A., Foretz, M., Viollet, B., 2011. Antagonistic control of muscle cell size by AMPK and mTORC1. Cell Cycle 10, 2640–2646.

Najumudeen, A.K., Jaiswal, A., Lectez, B., Oetken-Lindholm, C., Guzman, C., Siljamaki, E., Posada, I.M., Lacey, E., Aittokallio, T., Abankwa, D., 2016. Cancer stem cell drugs target K-ras signaling in a stemness context. Oncogene 35, 5248–5262.

Nassar, D., Blanpain, C., 2016. Cancer Stem Cells: Basic Concepts and Therapeutic Implications. Annu Rev. Pathol. 11, 47–76.

Norris, S.R., Nunez, M.F., Verhey, K.J., 2015. Influence of fluorescent tag on the motility properties of kinesin-1 in single-molecule assays. Biophys. J. 108, 1133–1143.

Okutachi, S., Manoharan, G.B., Kiriazis, A., Laurini, C., Catillon, M., McCormick, F., Yli-Kauhaluoma, J., Abankwa, D., 2021. A Covalent Calmodulin Inhibitor as a Tool to Study Cellular Mechanisms of K-Ras-Driven Stemness. Front Cell Dev. Biol. 9, 665673.

Olguin, H.C., Olwin, B.B., 2004. Pax-7 up-regulation inhibits myogenesis and cell cycle progression in satellite cells: a potential mechanism for self-renewal. Dev. Biol. 275, 375–388.

Olson, E.N., Spizz, G., Tainsky, M.A., 1987. The oncogenic forms of N-ras or H-ras prevent skeletal myoblast differentiation. Mol. Cell Biol. 7, 2104–2111.

Pal, R., Mamidi, M.K., Das, A.K., Bhonde, R., 2012. Diverse effects of dimethyl sulfoxide (DMSO) on the differentiation potential of human embryonic stem cells. Arch. Toxicol. 86, 651–661.

Parisi, B., Sunnen, M., Chippalkatti, R., Abankwa, D.K., 2023. A flow-cytometry-based pipeline for the rapid quantification of C2C12 cell differentiation. STAR Protoc. 4, 102637.

Pavic, K., Chippalkatti, R., Abankwa, D., 2022. Drug targeting opportunities en route to Ras nanoclusters. Adv. Cancer Res 153 63–99.

Post, Y., Clevers, H., 2019. Defining Adult Stem Cell Function at Its Simplest: The Ability to Replace Lost Cells through Mitosis. Cell Stem Cell 25, 174–183.

Prior, I.A., Hood, F.E., Hartley, J.L., 2020. The Frequency of Ras Mutations in Cancer. Cancer Res 80, 2969–2974.

Punekar, S.R., Velcheti, V., Neel, B.G., Wong, K.K., 2022. The current state of the art and future trends in RAS-targeted cancer therapies. Nat. Rev. Clin. Oncol. 19, 637–655.

Quinlan, M.P., Quatela, S.E., Philips, M.R., Settleman, J., 2008. Activated Kras, but not Hras or Nras, may initiate tumors of endodermal origin via stem cell expansion. Mol. Cell Biol. 28, 2659–2674.

Rabara, D., Tran, T.H., Dharmaiah, S., Stephens, R.M., McCormick, F., Simanshu, D.K., Holderfield, M., 2019. KRAS G13D sensitivity to neurofibromin-mediated GTP hydrolysis. Proc. Natl. Acad. Sci. USA 116, 22122–22131.

Rauen, K.A., 2013. The RASopathies. Annu Rev. Genom. Hum. Genet 14, 355–369.

Rommel, C., Clarke, B.A., Zimmermann, S., Nunez, L., Rossman, R., Reid, K., Moelling, K., Yancopoulos, G.D., Glass, D.J., 1999. Differentiation stage-specific inhibition of the Raf-MEK-ERK pathway by Akt. Science 286, 1738–1741.

Scheffzek, K., Ahmadian, M.R., Kabsch, W., Wiesmuller, L., Lautwein, A., Schmitz, F., Wittinghofer, A., 1997. The Ras-RasGAP complex: structural basis for GTPase activation and its loss in oncogenic Ras mutants. Science 277, 333–338.

Schmick, M., Kraemer, A., Bastiaens, P.I., 2015. Ras moves to stay in place. Trends Cell Biol. 25, 190–197.

Schubbert, S., Zenker, M., Rowe, S.L., Boll, S., Klein, C., Bollag, G., van der Burgt, I., Musante, L., Kalscheuer, V., Wehner, L.E., Nguyen, H., West, B., Zhang, K.Y., Sistermans, E., Rauch, A., Niemeyer, C.M., Shannon, K., Kratz, C.P., 2006. Germline KRAS mutations cause Noonan syndrome. Nat. Genet 38, 331–336.

She, X., Gao, Y., Zhao, Y., Yin, Y., Dong, Z., 2021. A high-throughput screen identifies inhibitors of lung cancer stem cells. Biomed. Pharm. 140, 111748.

Sherman, S.P., Pyle, A.D., 2013. Small molecule screening with laser cytometry can be used to identify pro-survival molecules in human embryonic stem cells. PLoS One 8, e54948.

Shern, J.F., Chen, L., Chmielecki, J., Wei, J.S., Patidar, R., Rosenberg, M., Ambrogio, L., Auclair, D., Wang, J., Song, Y.K., Tolman, C., Hurd, L., Liao, H., Zhang, S., Bogen, D., Brohl, A.S., Sindiri, S., Catchpoole, D., Badgett, T., Getz, G., Mora, J., Anderson, J.R., Skapek, S.X., Barr, F.G., Meyerson, M., Hawkins, D.S., Khan, J., 2014. Comprehensive genomic analysis of rhabdomyosarcoma reveals a landscape of alterations affecting a common genetic axis in fusion-positive and fusion-negative tumors. Cancer Discov. 4, 216–231.

Shu, L., Houghton, P.J., 2009. The mTORC2 complex regulates terminal differentiation of C2C12 myoblasts. Mol. Cell Biol. 29, 4691–4700.

Siddiqui, F.A., Vukic, V., Salminen, T.A., Abankwa, D., 2021. Elaiophylin Is a Potent Hsp90/ Cdc37 Protein Interface Inhibitor with K-Ras Nanocluster Selectivity. Biomolecules 11.

Siljamaki, E., Abankwa, D., 2016. SPRED1 Interferes with K-ras but Not H-ras Membrane Anchorage and Signaling. Mol. Cell Biol. 36, 2612–2625.

Simanshu, D.K., Nissley, D.V., McCormick, F., 2017. RAS Proteins and Their Regulators in Human Disease. Cell 170, 17–33.

Skapek, S.X., Ferrari, A., Gupta, A.A., Lupo, P.J., Butler, E., Shipley, J., Barr, F.G., Hawkins, D.S., 2019. Rhabdomyosarcoma. Nat. Rev. Dis. Prim. 5 (1).

Skoulidis, F., Li, B.T., Dy, G.K., Price, T.J., Falchook, G.S., Wolf, J., Italiano, A., Schuler, M., Borghaei, H., Barlesi, F., Kato, T., Curioni-Fontecedro, A., Sacher, A., Spira, A., Ramalingam, S.S., Takahashi, T., Besse, B., Anderson, A., Ang, A., Tran, Q., Mather, O., Henary, H., Ngarmchamnanrith, G., Friberg, G., Velcheti, V., Govindan, R., 2021. Sotorasib for Lung Cancers with KRAS p.G12C Mutation. N. Engl. J. Med 384, 2371–2381.

Steffen, C.L., Kaya, P., Schaffner-Reckinger, E., Abankwa, D., 2023. Eliminating oncogenic RAS: back to the future at the drawing board. Biochem Soc. Trans.

Stevenson, D.A., Allen, S., Tidyman, W.E., Carey, J.C., Viskochil, D.H., Stevens, A., Hanson, H., Sheng, X., Thompson, B.A., Okumura, M.J., Reinker, K., Johnson, B., Rauen, K.A., 2012. Peripheral muscle weakness in RASopathies. Muscle Nerve 46, 394–399.

Stevenson, D.A., Yang, F.C., 2011. The musculoskeletal phenotype of the RASopathies. Am. J. Med Genet C. Semin Med Genet 157C, 90–103.

Stowe, I.B., Mercado, E.L., Stowe, T.R., Bell, E.L., Oses-Prieto, J.A., Hernandez, H., Burlingame, A.L., McCormick, F., 2012. A shared molecular mechanism underlies the human rasopathies Legius syndrome and Neurofibromatosis-1. Genes Dev. 26, 1421–1426.

Tidyman, W.E., Goodwin, A.F., Maeda, Y., Klein, O.D., Rauen, K.A., 2022. MEK-inhibitor-mediated rescue of skeletal myopathy caused by activating Hras mutation in a Costello syndrome mouse model. Dis. Model Mech. 15.

Tsai, F.D., Lopes, M.S., Zhou, M., Court, H., Ponce, O., Fiordalisi, J.J., Gierut, J.J., Cox, A. D., Haigis, K.M., Philips, M.R., 2015. K-Ras4A splice variant is widely expressed in cancer and uses a hybrid membrane-targeting motif. Proc. Natl. Acad. Sci. USA 112, 779–784.

Tsherniak, A., Vazquez, F., Montgomery, P.G., Weir, B.A., Kryukov, G., Cowley, G.S., Gill, S., Harrington, W.F., Pantel, S., Krill-Burger, J.M., Meyers, R.M., Ali, L., Goodale, A., Lee, Y., Jiang, G., Hsiao, J., Gerath, W.F.J., Howell, S., Merkel, E., Ghandi, M., Garraway, L.A., Root, D.E., Golub, T.R., Boehm, J.S., Hahn, W.C., 2017. Defining a Cancer Dependency Map. Cell 170, 564–576 e516.

Vasta, J.D., Peacock, D.M., Zheng, Q., Walker, J.A., Zhang, Z., Zimprich, C.A., Thomas, M.R., Beck, M.T., Binkowski, B.F., Corona, C.R., Robers, M.B., Shokat, K.M., 2022. KRAS is vulnerable to reversible switch-II pocket engagement in cells. Nat. Chem. Biol. 18, 596–604.

Velica, P., Bunce, C.M., 2011. A quick, simple and unbiased method to quantify C2C12 myogenic differentiation. Muscle Nerve 44, 366–370.

Wakioka, T., Sasaki, A., Kato, R., Shouda, T., Matsumoto, A., Miyoshi, K., Tsuneoka, M., Komiya, S., Baron, R., Yoshimura, A., 2001. Spred is a Sprouty-related suppressor of Ras signalling. Nature 412, 647–651.

Wall, V.E., Garvey, L.A., Mehalko, J.L., Procter, L.V., Esposito, D., 2014. Combinatorial assembly of clone libraries using site-specific recombination. Methods Mol. Biol. 1116 193–208.

Wang, M.T., Holderfield, M., Galeas, J., Delrosario, R., To, M.D., Balmain, A., McCormick, F., 2015. K-Ras Promotes Tumorigenicity through Suppression of Non-canonical Wnt Signaling. Cell 163, 1237–1251.

Wang, X., Allen, S., Blake, J.F., Bowcut, V., Briere, D.M., Calinisan, A., Dahlke, J.R., Fell, J.B., Fischer, J.P., Gunn, R.J., Hallin, J., Laguer, J., Lawson, J.D., Medwid, J., Newhouse, B., Nguyen, P., O'Leary, J.M., Olson, P., Pajk, S., Rahbaek, L., Rodriguez, M., Smith, C.R., Tang, T.P., Thomas, N.C., Vanderpool, D., Vigers, G.P., Christensen, J.G., Marx, M.A., 2022. Identification of MRTX1133, a Noncovalent, Potent, and Selective KRAS(G12D) Inhibitor. J. Med Chem. 65, 3123–3133.

Weiswald, L.B., Bellet, D., Dangles-Marie, V., 2015. Spherical cancer models in tumor biology. Neoplasia 17, 1–15.

Weyman, C.M., Wolfman, A., 1998. Mitogen-activated protein kinase kinase (MEK) activity is required for inhibition of skeletal muscle differentiation by insulin-like growth factor 1 or fibroblast growth factor 2. Endocrinology 139, 1794–1800.

Whyte, D.B., Kirschmeier, P., Hockenberry, T.N., Nunez-Oliva, I., James, L., Catino, J.J., Bishop, W.R., Pai, J.K., 1997. K- and N-Ras are geranylgeranylated in cells treated with farnesyl protein transferase inhibitors. J. Biol. Chem. 272, 14459–14464.

Xu, Q., Wu, Z., 2000. The insulin-like growth factor-phosphatidylinositol 3-kinase-Akt signaling pathway regulates myogenin expression in normal myogenic cells but not in rhabdomyosarcoma-derived RD cells. J. Biol. Chem. 275, 36750–36757.

Yablonka-Reuveni, Z., Rivera, A.J., 1994. Temporal expression of regulatory and structural muscle proteins during myogenesis of satellite cells on isolated adult rat fibers. Dev. Biol. 164, 588–603.

Yan, W., Markegard, E., Dharmaiah, S., Urisman, A., Drew, M., Esposito, D., Scheffzek, K., Nissley, D.V., McCormick, F., Simanshu, D.K., 2020. Structural Insights into the SPRED1-Neurofibromin-KRAS Complex and Disruption of SPRED1-Neurofibromin Interaction by Oncogenic EGFR. Cell Rep. 32, 107909.

Yin, H., Price, F., Rudnicki, M.A., 2013. Satellite cells and the muscle stem cell niche. Physiol. Rev. 93, 23–67.

Yohe, M.E., Gryder, B.E., Shern, J.F., Song, Y.K., Chou, H.C., Sindiri, S., Mendoza, A., Patidar, R., Zhang, X., Guha, R., Butcher, D., Isanogle, K.A., Robinson, C.M., Luo, X., Chen, J.Q., Walton, A., Awasthi, P., Edmondson, E.F., Difilippantonio, S., Wei, J.S., Zhao, K., Ferrer, M., Thomas, C.J., Khan, J., 2018. MEK inhibition induces MYOG

and remodels super-enhancers in RAS-driven rhabdomyosarcoma. Sci. Transl. Med 10.
Yoon, M.S., 2017. mTOR as a Key regulator in maintaining skeletal muscle mass. Front Physiol. 8, 788.
Yoshida, N., Yoshida, S., Koishi, K., Masuda, K., Nabeshima, Y., 1998. Cell heterogeneity upon myogenic differentiation: down-regulation of MyoD and Myf-5 generates 'reserve cells. J. Cell Sci. 111 (Pt 6), 769–779.
Zembruski, N.C., Stache, V., Haefeli, W.E., Weiss, J., 2012. 7-Aminoactinomycin D for apoptosis staining in flow cytometry. Anal. Biochem 429, 79–81.